

Colloquium: The transport properties of graphene: An introduction

N. M. R. Peres

Physics Department and CFUM,
University of Minho,
P-4710-057, Braga,
Portugal

An introduction to the transport properties of graphene combining experimental results and theoretical analysis is presented. In the theoretical description simple intuitive models are used to illustrate important points on the transport properties of graphene. The concept of chirality, stemming from the massless Dirac nature of the low energy physics of the material, is shown to be instrumental in understanding its transport properties: the conductivity minimum, the electronic mobility, the effect of strain, the weak (anti-)localization, and the optical conductivity.

PACS numbers: 81.05.ue,72.80.Vp,78.67.Wj

CONTENTS

I. Introduction	1
II. The energy spectrum of graphene and the emergence of Dirac electrons	2
III. Conductivity and conductance of graphene at the Dirac point	4
A. Sources of disorder	4
B. Calculation of the conductivity minimum for bulk graphene due to disorder	6
C. Calculation of the conductivity minimum for pristine graphene ribbons	7
D. Puddles	9
IV. The transport properties of graphene at finite electronic density	10
A. The dependence of the conductivity on the gate voltage	10
B. Partial-wave description of resonant scatterers	12
C. Partial-wave description of Coulomb scatterers	14
D. Transport across a strained region: A way of generating a transport gap	16
V. Quantum corrections to the Drude conductivity	19
A. Weak localization in a normal metal	19
B. Weak localization in graphene	20
VI. The optical conductivity of graphene in the infrared to visible range of the spectrum	22
A. Graphene as a transparent membrane	22
B. The optical conductivity of neutral graphene	23
C. The optical conductivity of gated graphene	25
VII. Conclusions	26
Acknowledgments	26
References	26

I. INTRODUCTION

For a long time, theorists and experimentalists alike have considered the existence of a true two-dimensional (2D) material, having the thickness of a single atom –

a one atom thick membrane – to be impossible. The reasoning behind this statement relies on the fact that both finite temperature and quantum fluctuations conspire to destroy the otherwise perfect 2D structure of the hypothetical material. These fluctuations, originated from atomic vibrations perpendicular to the plane of the material, would preclude the existence of a true flat phase and concomitantly the existence of such a system.

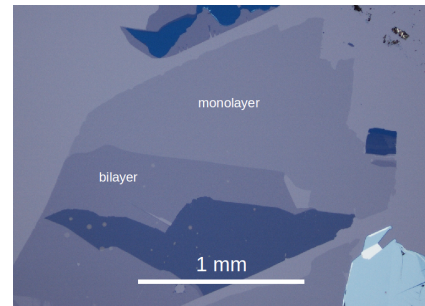


Figure 1 (Color online) An optical image of a graphene flake, obtained from the exfoliation of graphite, with an area of $\lesssim 1 \text{ mm}^2$, on top of a silicon oxide wafer (courtesy of P. Blake).

Nevertheless, in 2004, a group led by A. K. Geim, from the University of Manchester, U.K., isolated such a 2D material (Novoselov *et al.*, 2004, 2005b). Under the name of graphene, this new material is an allotropic form of carbon, with the atoms arranged in a 2D honeycomb lattice. The reason for the success lies on the isolation method. The developed method permitted one to isolate the 2D material on top of a 300 nm thick wafer of silicon oxide. The weak van der Waals interaction induces adhesion between graphene and the wafer, and once on top of the wafer, it is possible to move about the 2D material, transferring it from one substrate to another, or even having it suspended over a trench, supported from one side (Booth *et al.*, 2008). In the production method, graphite plays a key role, since this 3D material is itself made of stacked

graphene planes (bonded by van der Waals forces). The ingenuity of the method was then to find a way of peeling a single layer of graphene out of graphite (Novoselov *et al.*, 2004, 2005b). Up to this date, the exfoliation of graphite can produce graphene crystallites as large as $\sim 1 \text{ mm}^2$ (see Fig. 1). The study of graphene became, since 2004, an active field of research in condensed matter, which holds many promises (Castro Neto, 2010; Castro Neto *et al.*, 2006; Fuhrer *et al.*, 2010; Geim, 2009; Geim and Kim, 2008; Geim and MacDonald, 2007; Geim and Novoselov, 2007; Katsnelson, 2007; Peres, 2009; Service, 2009).

Being the first truly 2D material, it is natural to ask how its properties differ from those of more conventional systems, such as the 2D electron gas in the inversion layer of an ordinary semiconductor. The current efforts in graphene research have focused on the interplay among elastic, thermal, chemical, and electronic properties of the material, with a special emphasis on charge and heat transport, and on optical properties. The need for a deep understanding of the transport properties of graphene is obvious, since the material is a potential candidate for incorporating the future generation of nanoelectronic and nanophotonic devices (Blake *et al.*, 2008; Liao *et al.*, 2010; Lin *et al.*, 2010; Mueller *et al.*, 2010; Schwierz, 2010; Xia *et al.*, 2009). Also in biophysics, graphene is finding new applications (Lu *et al.*, 2010; Schneider *et al.*, 2010; Wu *et al.*, 2010). Additionally, and of no less importance, graphene provides a realm for the emergence of new and exciting physics.

In the field of electronic applications, faster electronics requires smaller devices, in particular because at the nanoscale it may be possible for the electrons to travel across some of the components of a device almost unimpeded. In a normal conductor, one of the sources of electrical resistance is scattering of electrons by impurities and defects (and at room temperature, also by phonons). A measure of the effect of impurities on the electronic transport is the mean free path ℓ (the average distance traveled by an electron between two consecutive collisions), which in a material with high degree of purity and with small dimensions can be larger than the typical length of the system L_x leading, in these circumstances, to what is called ballistic transport (in this regime the current becomes spatially non-uniform). It just happens that in graphene ℓ can be as large as $1 \mu\text{m}$ (Bolotin *et al.*, 2008a; Novoselov *et al.*, 2004), putting graphene into to the ballistic regime, since the typical size of graphene-based field effect transistors is $L_x \sim 0.25\text{-}0.5 \mu\text{m}$ (Du *et al.*, 2008).

The first ground breaking publications of the Manchester's group (Novoselov *et al.*, 2004, 2005b) not only made the method of isolating graphene immediately public, but also established the major relevant problems in graphene transport: the ambipolar field effect (see Fig. 9), the independence of the electronic mobility upon the

gate voltage, the large electronic mean free path, the conductivity minimum and the absence of Anderson localization (Bardarson *et al.*, 2007), the magneto-resistance and the chiral quantum Hall effect (Novoselov *et al.*, 2005a; Zhang *et al.*, 2005). These topics still orient much of the research in graphene physics at present.

Since the publication of a comprehensive review on the theoretical properties of graphene (Castro Neto *et al.*, 2009), there has been additional relevant contributions to experimental and theoretical studies of its transport properties. In this Colloquium, we present an update on the experimental and theoretical developments in this fast growing subfield of graphene research, at a level appropriate to graduate students entering the field.

II. THE ENERGY SPECTRUM OF GRAPHENE AND THE EMERGENCE OF DIRAC ELECTRONS

As stated, graphene is a 2D material made solely of carbon atoms, arranged in a hexagonal lattice such as that shown in Fig. 2. There are five vectors represented in Fig. 2: the three next-nearest neighbors vectors δ_i ($i = 1, 2, 3$), and the primitive cell vectors \mathbf{a}_1 and \mathbf{a}_2 . We further note that the hexagonal lattice is made of two inter-penetrating triangular Bravais lattices. Therefore, the effective model describing the low-energy physics of graphene has to keep track of the two atoms per unit cell, characteristic of the honeycomb lattice. Electrons in graphene can be described by a tight-binding Hamiltonian reading (spin index omitted)

$$H = -t \sum_{n, \delta_i} |A, \mathbf{R}_n\rangle \langle \mathbf{R}_n + \delta_i, B| + \text{H. c.}, \quad (1)$$

where $|A, \mathbf{R}_n\rangle$ represents the Wannier state at the unit cell \mathbf{R}_n , and the equivalent definition holds for $|B, \mathbf{R}_n + \delta_i\rangle$; t is the hopping energy. This Hamiltonian describes the motion of electrons in the π -orbitals of the material, made from the hybridization of the atomic $2p_z$ orbitals, and includes both low-energy and high-energy electron states. The calculation of the electronic energy spectrum of graphene proceeds by introducing, in Eq. (1), the Fourier representation of the Wannier states in terms of the Bloch states of momentum \mathbf{k} ; the spectrum then reads (Castro Neto *et al.*, 2009; Wallace, 1947)

$$E(\mathbf{k}) = \pm t |1 + e^{i\mathbf{k}\cdot\mathbf{a}_1} + e^{i\mathbf{k}\cdot\mathbf{a}_2}|. \quad (2)$$

It is immediately obvious that the band structure of the π -electrons is composed of two bands, one at negative energies (a hole band) and the other at positive ones (a particle band). In the Brillouin zone there are two special, non-equivalent (i.e. not connected by a reciprocal lattice vector), wave numbers, termed \mathbf{K} and \mathbf{K}' , and shown in Fig. 2. The transport properties of graphene are mostly determined by the nature of the spectrum

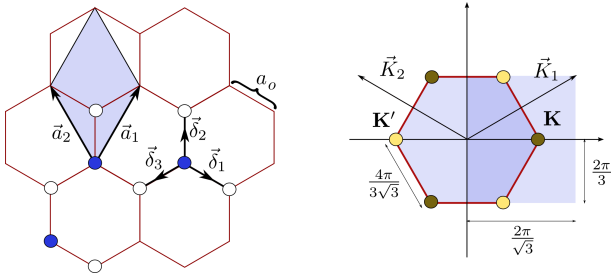


Figure 2 (Color online) Real space lattice and Brillouin zone of graphene. **Left:** The hexagonal lattice of graphene, with the nearest neighbor δ_i and the primitive \mathbf{a}_i vectors depicted. The area of the primitive cell is $A_c = 3\sqrt{3}a_0^2/2 \simeq 5.1 \text{ \AA}^2$, and $a_0 \simeq 1.4 \text{ \AA}$. **Right:** The Brillouin zone of graphene, with the Dirac points \mathbf{K} and \mathbf{K}' indicated. Close to these points, the dispersion of graphene is conical and the density of states is proportional to the absolute value of the energy.

around these two points. Close to \mathbf{K} and \mathbf{K}' the dispersion, Eq. (2), is conical, and given by $E(\mathbf{k}) = \pm v_F \hbar k$, with $v_F = 3ta_0/2\hbar$, where k is the momentum measured relatively to either \mathbf{K} or \mathbf{K}' , depending on the position of the cone in the Brillouin zone. Using the widely accepted value of $t \simeq -2.7 \text{ eV}$ for the hopping (in reality the values of t vary in the literature, spanning the interval from -2.7 to -3.1 eV) we obtain $v_F \lesssim 10^6 \text{ m/s}$. The experimental studies are consistent in obtaining $v_F \simeq 1.1 \times 10^6 \text{ m/s}$ (Jiang *et al.*, 2007; Novoselov *et al.*, 2005a; Zhang *et al.*, 2008, 2005). A direct measurement of the Dirac spectrum in graphene has recently been obtained using angle-resolved photo-emission spectroscopy (Sprinkle *et al.*, 2009). Since each carbon atom (electronic configuration $1s^2 2s^2 2p^2$) hybridizes with its three nearest neighbors according to the hybrid orbitals sp^2 , there is one electron left in the p_z orbital. Therefore, the system is half filled, with the important consequence that the low-energy physics is controlled by the spectrum close to the \mathbf{K} and \mathbf{K}' points. Many of the new and exciting properties of graphene stem from this fact. The vicinities of these two points are also referred to as the two valleys of the electronic spectrum of graphene.

The spectrum $E(\mathbf{k}) = \pm v_F \hbar k$ is formally equivalent to that obtained from solving the 2D massless Dirac equation. Indeed, it is easy to show (Castro Neto *et al.*, 2009; Semenoff, 1984) that close to the \mathbf{K} point the effective Hamiltonian for the electrons in graphene has the form

$$H_{\mathbf{K}} = v_F \boldsymbol{\sigma} \cdot \mathbf{p}, \quad (3)$$

whereas close to \mathbf{K}' , the Hamiltonian is obtained from Eq. (3) by making the transformation $H_{\mathbf{K}'} = -H_{\mathbf{K}}$. The operator $\boldsymbol{\sigma}$ is written in terms of the Pauli matrices as $\boldsymbol{\sigma} = (\sigma_x, \sigma_y)$, and \mathbf{p} is the momentum operator. Computing the eigenvalues of the Hamiltonian (3), the conical spectrum indicated above is immediately obtained. We stress that $\boldsymbol{\sigma}$ does not represent real electronic spin; it is instead a formal way of taking into account the two

carbon atoms per unit cell in graphene, as we have anticipated above. For this reason, $\boldsymbol{\sigma}$ is termed pseudo-spin. The density of states associated with the conical dispersion of electrons in graphene is computed by determining the number of states per unit cell in the Brillouin zone $N(E)$ up to the momentum k . Taking into account contributions from states near \mathbf{K} and \mathbf{K}' points, we obtain $N(E) = k^2 A_c / (2\pi)$, from which the density of states $\rho(E)$ per spin and per unit cell is given by $\rho(E) \equiv dN(E)/dE = 2|E|/(\pi\sqrt{3}t^2)$, and the primitive cell area, A_c , is defined in the caption of Fig. 2. The linear dependence of the density of states on energy is one of the fingerprints of massless Dirac electrons. For neutral graphene, the Fermi energy is zero. Therefore, the density of states vanishes in this case.

The electronic linear spectrum and the chiral nature of the electron's wave function (see below) make electronic behavior in graphene quite unique, and are responsible for the remarkable properties of this material. Since $\boldsymbol{\sigma} \cdot \mathbf{p}|\psi\rangle = \pm p|\psi\rangle$, then the operator $\hat{h} = \boldsymbol{\sigma} \cdot \mathbf{p}/p$ has only two eigenvalues ± 1 . The operator \hat{h} is known as the helicity operator, and has the following physical interpretation: in an energy eigenstate, the pseudo-spin $\boldsymbol{\sigma}$ is either parallel or anti-parallel to the momentum \mathbf{p} . In the \mathbf{K} valley, electrons have positive helicity and holes have negative helicity; in \mathbf{K}' the opposite happens. The helicity (or chirality) of electrons in graphene is responsible for the Klein tunneling effect (Beenakker, 2008; Cheianov and Fal'ko, 2006; Katsnelson *et al.*, 2006), observed recently in graphene heterojunctions (Stander *et al.*, 2009; Young and Kim, 2009). We then see (and at odds to high-energy neutrino physics) that massless Dirac electrons in graphene come with both right and left chirality: parity is a symmetry of graphene. In Fig. 3 we show, in simple terms, the origin of the Klein tunneling effect: the probability of electronic transmission through a potential barrier is equal to 1, for head-on collisions; it is said that backscattering is suppressed.

We should note that chirality is not, however, an exact symmetry of the problem. This occurs because the spectrum of graphene is not exactly linear at all energies. The deviation from the perfect massless Dirac behavior is known as trigonal warping (McCann *et al.*, 2006; Narozhny, 2007), and starts playing a role for energies $E \gtrsim 1 \text{ eV}$. We remark, however, that trigonal warping might be important for observation of weak localization at energies much lower than 1 eV (see Sec. V.B).

The solution of the eigenproblem $H_{\mathbf{K}}|\psi\rangle = E|\psi\rangle$ is easily obtained by recognizing its formal equivalence to that of a real spin in a magnetic field (Castro Neto *et al.*, 2009), with the wave function reading

$$|\psi_{\pm}\rangle = \frac{1}{\sqrt{2}} \begin{pmatrix} e^{-i\theta(\mathbf{k})/2} \\ \pm e^{i\theta(\mathbf{k})/2} \end{pmatrix} e^{i\mathbf{k}\cdot\mathbf{r}} \equiv u_{\pm}(\mathbf{k})e^{i\mathbf{k}\cdot\mathbf{r}}, \quad (4)$$

and $\theta(\mathbf{k}) = \arctan(k_y/k_x)$. Since the eigenproblem we have just solved is formally identical to a spin one-half

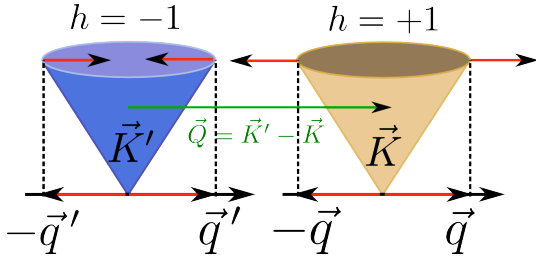


Figure 3 (Color online) At the \mathbf{K} valley, electrons have positive helicity, $h = 1$, whereas at the \mathbf{K}' one, the helicity is negative ($\mathbf{Q} = \mathbf{K}' - \mathbf{K}$ represents the transferred momentum when a scattering event between the valleys takes place). In a head-on collision of the electron on a potential barrier, the backscattered electron has to change its momentum from \mathbf{q} to $-\mathbf{q}$. For such a head-on collision (taken here along the x -direction), \hat{h} is a constant of motion, with eigenvalue $+1$, but backscattering would imply a modification of this eigenvalue to -1 . This, however, cannot be, because \hat{h} is a conserved quantity, then the transmission probability through the barrier, for such type of collision, has to be one. Thus, backscattering is suppressed for intra-valley scattering events. On the other hand, electrons in the \mathbf{K}' and \mathbf{K} valleys have opposite chirality, thus inter-valley backscattering can take place (if the potential is short range), since in this case the eigenvalue of \hat{h} does not change sign. This discussion will be of importance for Sec. V.B.

in a magnetic field, the spinors change sign upon the transformation $\theta(\mathbf{k}) \rightarrow \theta(\mathbf{k}) + 2\pi$, as dictated by the spin-statistics theorem.

The first striking consequence of the chiral nature of electrons in graphene was the observation of the chiral quantum Hall effect (Novoselov *et al.*, 2005a; Zhang *et al.*, 2005), where the Hall conductivity is quantized as $\sigma_{xy} = 2e^2(1 + 2n)/h$, with $n = 1, 2, \dots$ (Gusynin and Sharapov, 2005; Peres *et al.*, 2006). The quantization rule follows from the nature of the Landau levels of Dirac electrons (Johnson and Lippmann, 1949; Nieto and Taylor, 1985; Peres and Castro, 2007; Rabi, 1928) combined with the existence of the two valleys in graphene.

The application of the chiral quantum Hall effect to metrology, in defining the resistance standard (Delahaye and Jeckelmann, 2003), has clear advantages over the usual quantum Hall effect in the 2D electron gas, since the same experimental accuracy on the quantization of the Hall resistance can be achieved at higher temperatures (Giesbers *et al.*, 2008; Poirier and Schopfe, 2010; Tzalenchuk *et al.*, 2010). At a temperature of 300 mK, the accuracy of the quantum Hall resistance quantization has been shown to be of 3 parts per billion, in monolayer epitaxial graphene (Poirier and Schopfe, 2010; Tzalenchuk *et al.*, 2010). Also, the quantum Hall effect in graphene has been observed at room temperature (Novoselov *et al.*, 2007) and recently in epitaxial graphene as well (Wu *et al.*, 2009), which can be produced in quasi-free standing form (Riedl *et al.*, 2009).

Electron-electron interactions play no role in the half-integer or chiral quantum Hall effect. On the other hand, they are a crucial ingredient in the explanation of the fractional quantum Hall effect. During the first few years of graphene quantum research, effects of electron-electron interactions have been elusive, but the recent observation of the $1/3$ fractional Hall plateau (Bolotin *et al.*, 2009; Du *et al.*, 2009; Morpurgo, 2009), brings them to the forefront this active research area. It is a remarkable experimental fact that the fractional quantum Hall effect in graphene can be observed at magnetic fields of 2 T and persists up to a temperature of 20 K, for fields of 12 T.

Using the results introduced above, we proceed to the discussion of several topics on electronic transport in graphene.

III. CONDUCTIVITY AND CONDUCTANCE OF GRAPHENE AT THE DIRAC POINT

As discussed in Sec. II, undoped graphene has its Fermi energy at the Dirac point, where the material has a vanishing density of states. This would naively suggest that the conductivity of undoped graphene should be zero. However, experiments challenge ones intuition and show a finite conductivity at zero energy (i. e., at the neutrality or Dirac point). An example of a conductivity curve of graphene is shown in Fig. 8, where we see that the experimental conductivity minimum, at $V_g = 0$, is of the order of $\sim 4e^2/h$ (horizontal dashed line). Values of the conductivity minimum for several devices are given in Fig. 5. The existence of a conductivity minimum in graphene is also referred to as quantum-limited resistivity.

A. Sources of disorder

As in any other metallic system, the electronic mobility in graphene is hindered by disorder. The sources of disorder in graphene can vary, and can be due to adsorbed atoms (for example hydrogen) or molecules (for example hydrocarbons), extended defects, such as folded regions (wrinkles), vacancies, and topological defects [such as of Stone-Wales type, specially at the edges (Huang *et al.*, 2009)]. Interestingly enough, in some particular cases, an extended defect in graphene can act as a 1D conducting channel (Lahiri *et al.*, 2010). In addition, the system has a certain amount of rippling (random strain) (Katsnelson and Geim, 2008; Meyer *et al.*, 2007), so it is not a perfect planar lattice, and it has rough edges, which can exhibit scrolling (Fogler *et al.*, 2010). We should note that, although the formation of vacancies is energetically unfavorable, the existence of adatoms and adsorbed hydrocarbons is likely, originating from the isolation method and exposure to the environment. Such adsorbed atoms can

be imaged by transmission electron microscopy (Meyer *et al.*, 2008). Additionally, the electrostatic random potential at the surface of the silicon-oxide substrate acts as an additional scattering source, originated from charged impurities (Zhang *et al.*, 2009).

To a good practical approximation, an adsorbed hydrocarbon, when binding covalently to the $2p_z$ orbital of a given carbon atom of graphene, effectively removes the $2p_z$ electron from participating in the electric transport, by forming a σ -bond. Since the electron wave-function is spatially confined, the impurity can effectively act as a vacancy. This latter type of defects induce resonant states at, or close to, the Dirac point (see below).

Another way of looking at this problem is to consider that, say, an hydrogen atom when binding covalently (Katoch *et al.*, 2010) to a carbon atom in graphene changes locally the hybridization from pure sp_2 to partially sp_3 and creates, as before, a resonant impurity at that site (Castro Neto and Guinea, 2009; Robinson *et al.*, 2008). In this latter sense, both local potentials and adatoms have a similar effect (Stauber *et al.*, 2008a). The change of the chemical bonds from pure sp_2 to partially sp_3 adds an additional scattering effect originated from the enhancement of spin-orbit coupling (Castro Neto and Guinea, 2009).

Combined with charged scatterers, the resonant scattering mechanism is currently ascending as one of the dominant processes limiting the electronic mobility in graphene (Ni *et al.*, 2010).

The resonant scattering mechanism is easy to understand by considering a simple model. We add to the Hamiltonian (1) a contribution from an impurity binding covalently to a carbon atom at site $\mathbf{R}_n = 0$. Such a situation adds to the Hamiltonian a term of the form $H_{rs} = (V|\text{ad}\rangle\langle A, 0| + \text{H. c.}) + \epsilon_{\text{ad}}|\text{ad}\rangle\langle \text{ad}|$, where V is the hybridization between the adatom (or a carbon atom of a hydrocarbon molecule) and a given carbon atom of graphene, ϵ_{ad} is the relative (to graphene's carbon atoms) on-site energy of the electron in the adatom, and $|\text{ad}\rangle$ is the ket representing the state of the electron in the adatom. Taking the wave function to be of the form $|\psi\rangle = \sum_n [A(\mathbf{R}_n)|A, \mathbf{R}_n\rangle + B(\mathbf{R}_n + \boldsymbol{\delta}_2)|B, \mathbf{R}_n + \boldsymbol{\delta}_2\rangle] + C_{\text{ad}}|\text{ad}\rangle$, the Schrödinger equation at the site $\mathbf{R}_n = 0$ reads

$$EA(0) - VC_{\text{ad}} = -t[B(\boldsymbol{\delta}_1) + B(\boldsymbol{\delta}_2) + B(\boldsymbol{\delta}_3)], \quad (5)$$

$$(E - \epsilon_{\text{ad}})C_{\text{ad}} = VA(0). \quad (6)$$

Solving for C_{ad} , we obtain

$$-t[B(\boldsymbol{\delta}_1) + B(\boldsymbol{\delta}_2) + B(\boldsymbol{\delta}_3)] = EA(0) - \frac{V^2 A(0)}{E - \epsilon_{\text{ad}}}. \quad (7)$$

The resonant effect is included in the last term of Eq. (7), which represents a local potential of the form $V_{\text{eff}} = V^2/(E - \epsilon_{\text{ad}})$. Equation (7) contains two interesting regimes: (i) when $|E| \ll \epsilon_{\text{ad}}$, the adatom acts as an effective local potential of strength $g_{\text{eff}} = V^2/\epsilon_{\text{ad}}$. If g_{eff} is

large, the adatom acts roughly as an effective vacancy; a vacancy is characterized by $g_{\text{eff}} = \infty$; (ii) when $E \approx \epsilon_{\text{ad}}$, the hopping from the carbon atom at position $\mathbf{R}_n = 0$ to its nearest neighbors is suppressed [effectively we have $t \rightarrow (E - \epsilon_{\text{ad}})t$], and the adatom acts roughly and again as an effective vacancy at energies close to ϵ_{ad} . Therefore, either by inducing an effective local potential or by suppressing the nearby hopping we see that such mechanism increases the likelihood of an electron being trapped for a longer time in the vicinity of the adatom, thus generating a resonant state.

If $\epsilon_{\text{ad}} \simeq 0$, then the resonant states will be exactly at the Dirac point, and this is expected to happen for adsorbed hydrocarbon molecules. It is then the job of quantum chemical calculations to determine the value of the parameters ϵ_{ad} and V (Robinson *et al.*, 2008; Wehling *et al.*, 2009, 2010). Recently obtained typical values are $V \sim 2t \sim 5$ eV and $\epsilon_{\text{ad}} \sim -0.2$ (Wehling *et al.*, 2010), leading to $g_{\text{eff}} \sim 100$ eV, a rather strong on-site potential. Finally, the calculation of the transport properties for such a model can be performed using the T -matrix approach (Peres *et al.*, 2007a, 2009b; Robinson *et al.*, 2008). Its derivation is elementary, using the simple model described above. It is well known that the T matrix for a local potential of intensity v_0 reads (Bena and Kivelson, 2005; Peres *et al.*, 2006) $T(E) = v_0[1 - v_0\bar{G}_R(E)]^{-1}$. Then, for an adatom we must have

$$T(E) = \frac{V_{\text{eff}}}{1 - V_{\text{eff}}\bar{G}_R(E)} = \frac{V^2}{E - \epsilon_{\text{ad}} - V^2\bar{G}_R(E)}. \quad (8)$$

Using Eq. (8), it is simple to compute the transport relaxation time $\tau(\epsilon_F)$ at the Fermi energy ϵ_F using $\hbar/\tau(\epsilon_F) = \pi n_i |T(\epsilon_F)|^2 \rho(\epsilon_F)$, where n_i is the concentration of impurities per unit cell. From the knowledge of $\tau(\epsilon_F)$, the conductivity of graphene follows from Boltzmann's transport equation (Ziman, 1979) (see Sec. VI.C). The function $\bar{G}_R(E)$ reads: $\bar{G}_R(E) = ED^{-2} \ln(E^2/D^2) - i\pi|E|/D^2$, with $D \simeq 3t$.

It has been theoretically predicted that, in addition to their scattering effect, monovalent adatoms in diluted concentrations can create a gap in graphene's spectrum, by a mechanism called *sublattice ordering* (Cheianov *et al.*, 2010). Superlattices of vacancies (or adatoms) have the same effect (Martinazzo *et al.*, 2010).

Midgap states (Jackiw, 1984) are also produced by a model of pure vacancies (Pereira *et al.*, 2006, 2008), as shown in Fig. 4, and if a nearest neighbor hopping ($t' \simeq 0.4$ eV) is included, the resonant states, while no longer at exactly the Dirac point, remain at energies close to it (Pereira *et al.*, 2006, 2008).

B. Calculation of the conductivity minimum for bulk graphene due to disorder

It is certainly difficult to model all the different types of disorder just mentioned in a single calculation. We for the moment ignore this complexity and assume that electrons in graphene move in a random potential of the form $V(\mathbf{r}) = v_0 \sum_{n=1}^{N_i} \delta(\mathbf{R}_n - \mathbf{r})$, where the position vectors \mathbf{R}_n are random, v_0 is the strength of the potential, and N_i is the number of scattering centers. This model can be seen in the worst case scenario as zero order description of the effect of impurities in graphene, although it has recently been used widely (Ando and Nakanishi, 1998; Ostrovsky *et al.*, 2006, 2007; Peres *et al.*, 2006; Suzuura and Ando, 2002; Zheng and Ando, 2002). In fact, for large v_0 this model mimics the resonant scatterers physics. In what follows, we determine the consequences of the above random potential on the minimum conductivity of graphene.

The usual approach to the calculation of the conductivity uses the Kubo-Greenwood formula, obtained from linear response theory (Mahan, 2000). The calculation proceeds in two steps (Peres *et al.*, 2006; Shon and Ando, 1998; Zheng and Ando, 2002): first, the single particle Green's function in the presence of the disordered potential is computed in a self-consistent manner; second the current-current correlation function is obtained in terms of the single particle Green's function. This method is known as the self-consistent Born approximation (SCBA). The final result of such calculation is a simple expression for the conductivity $\sigma(\epsilon_F)$ at the Fermi energy reading

$$\sigma(\epsilon_F) = \frac{4e^2}{\pi h} K(\epsilon_F), \quad (9)$$

where $K(\epsilon_F)$ is a dimensionless function (Peres *et al.*, 2006; Stauber *et al.*, 2008a); Eq. (9) holds true both at finite v_0 or when $v_0 \rightarrow \infty$; from here on we consider this latter regime only. Since we describe the transport at the Dirac point, we need the value of $K(\epsilon_F)$ at zero chemical potential, which turns out to be $K(0) \simeq 1$. This result is essentially insensitive to the concentration of impurities $n_i = N_i A_c / A$ (A is the area of the sample and n_i is the concentration of impurities per unit cell). The behavior of $K(0)$ as function of n_i is shown in the inset of Fig. 4; as stated, its value is 1. We have, therefore, obtained a universal value for the conductivity minimum of graphene $\sigma_{\min} = 4e^2 / (\pi h)$ independent of the impurity concentration, even if the concentration of impurities is a small number. Many have reached the same result using different approaches (Dóra *et al.*, 2008; Ziegler, 2007). A question naturally arises: How does one understand the result given by Eq. (9)? To that end, we compute the density of states of disordered graphene.

We have compared a calculation of the density of states as given by the SCBA with that given by an exact nu-

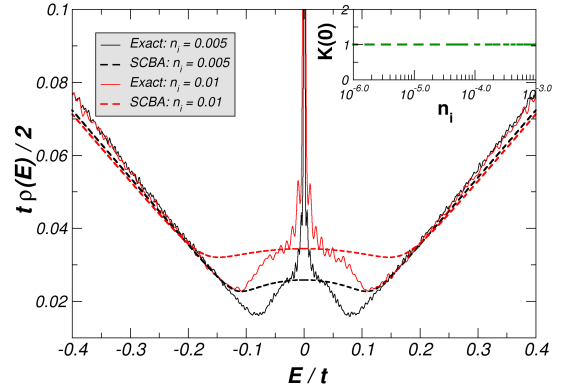


Figure 4 (Color online) Numerically exact density of states (solid lines), in the limit $v_0 \rightarrow \infty$, and the corresponding SCBA calculation (dashed lines), for the same impurity concentrations n_i . The maximum of the SCBA density of states, at $E = 0$, follows the rule $\rho(E) \simeq 0.2\sqrt{n_i} \text{ eV}^{-1}$. **Inset:** The function $K(0)$ is plotted for a range of impurity concentrations spanning three orders of magnitude. (The numerically exact calculations are courtesy of Vitor M. Pereira.)

merical method (Pereira *et al.*, 2006, 2008). In Fig. 4 we show two sets of calculations for the density of states close to the Dirac point ($E \sim 0$). Two features are clear from these calculations. First, the disorder only affects the DOS close to the Dirac point, rendering it finite; second the SCBA introduces a smoothing of DOS around $E \sim 0$, but its value essentially agrees with the exact one, except at energies very close to $E = 0$. The finite density of states close to the Dirac point is due to the wings of the resonant states forming at zero energy. The same behavior is seen in the local density of states around a single vacancy and in the corresponding scanning tunnelling microscopy current (Peres *et al.*, 2007a, 2009b).

The above comparison shows that the SCBA gives a reasonable description of the density of states close to the Dirac point, and this gives us a certain amount of confidence in the calculation of the conductivity $\sigma(\epsilon_F)$ based on the same approximation. A comment on the behavior of the numerical DOS close to zero energy is in order: the sharp feature at precisely $E = 0$ seen in the exact numerical solution arises from the presence of zero-energy quasilocalized modes, induced by the vacancies in the lattice (Pereira *et al.*, 2006, 2008). These localized states are clearly not captured by the SCBA.

In short, the finiteness of the conductivity at the Dirac point is a consequence of the finiteness of the DOS at $E \sim 0$ due to disorder, even when the concentration of impurities is small, since $K(0)$ is essentially constant over several orders of magnitude of impurity concentration. Furthermore, there is a strong criticism in the literature regarding the application of the SCBA approach to de-

scribe the physics at $\epsilon_F \simeq 0$ (Aleiner and Efetov, 2006), but not at finite ϵ_F , as long as weak localization effects are not important (see Sec. V.A).

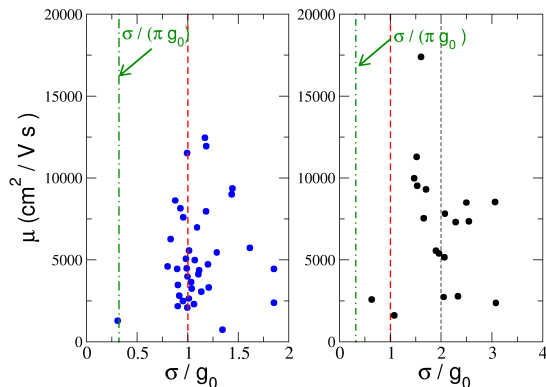


Figure 5 (Color online) The conductivity of graphene at the neutrality point. **Left:** conductivity minimum from the Manchester's group [Data from (Geim and Novoselov, 2007)]. **Right:** Conductivity minimum from the Columbia's group [data from (Tan *et al.*, 2007)] as function of the mobility of the devices. In both panels, several devices with different mobilities μ were measured. The mobility is defined as $\mu = \sigma(\epsilon_F)/(en)$, where n is the electron density, and is a measure of the amount of disorder in the system. The constant g_0 stands for twice the quantum of conductance, $2e^2/h \simeq 0.078$ (k Ω)⁻¹, and is represented by the dashed line. The dash-dotted line represents the value $\sigma = \sigma_{\min}$, obtained in Sec. III.B.

If one considers that the scattering centers are charged impurities, the conductivity of graphene, at the neutrality point, acquires the form (Fogler, 2009) $\sigma_{\min} = (e^2/h)c\mathcal{L}$ with $c = 0.5 \pm 0.05$ and \mathcal{L} the solution of the transcendent equation $\mathcal{L} = \ln(\mathcal{L}/4\alpha_g^{\text{eff}})$, where α_g^{eff} is the effective fine structure constant of graphene (see Sec. IV.C). This result for the conductivity minimum is different from that obtained for strong short-range scatterers.

Finally, the measured conductivity minimum, as shown in Fig. 5, has the same order of magnitude as that given by σ_{\min} , but is larger than this value and has a finite variance. It is important to note that the assessment of the transport properties of graphene at the neutrality (or Dirac) point can be strongly affected by the used probe geometry, the use of invasive contacts, or the lack of effective control on the sample's homogeneity (Blake *et al.*, 2009; Connolly *et al.*, 2010). These effects are responsible for the differences in the two sets of measurements given in Fig. 5.

C. Calculation of the conductivity minimum for pristine graphene ribbons

Graphene ribbons have been produced by different methods: etching of exfoliated graphene (Han *et al.*, 2007), using chemical reactions (Jiao *et al.*, 2010; Li *et al.*, 2008a), unzipping carbon nanotubes (Kosynkin *et al.*, 2009), and tailoring them by scanning tunneling microscope lithography (Tapasztó *et al.*, 2008). Much of the experimental challenge regarding the production of nanoribbons is related to the discovery of an experimental procedure allowing, in a systematic way, the engineering of ribbons with fixed widths and perfect edges, together with a detailed characterization of their transport properties (Han *et al.*, 2010).

The previous section addressed the problem of the conductivity minimum of graphene from the point of view of disorder. Another relevant problem is that of the transport properties of pristine ribbons, where electrons can be in the ballistic regime. The problem we are about to discuss is a rather interesting one, since electronic transport will proceed via evanescent modes, whereas in normal metals charge transport is associated with propagating states.

We show below, and also in this case, the system has a finite conductivity, which in some conditions has the same value we found in Sec. III.B, although the physical mechanism is different. The approach to the calculation of the conductivity of ribbons in the ballistic regime uses Landauer's formalism (Nazarov and Blanter, 2009), where the relevant quantity to be computed is the conductance of the system, which can formally take into account quantum interference effects, absent from the elementary Boltzmann's transport theory (but see Sec. V.A).

The measurements in bulk metals of dc-transport properties allows one obtain directly the resistance R of the sample, from which the linear conductance $G = 1/R$ can be determined. In bulk metals, we can define a material intrinsic quantity, the conductivity σ . Taking the example of a 2D system, we have $\sigma = GL_x/L_y$, where L_x and L_y are the longitudinal and transverse dimensions of the bulk sample, respectively. The conductivity is a well-defined quantity whenever the system is large enough, such that the electronic current is homogeneous and insensitive to variations of the impurities' position from sample to sample. In this regime the transport is well described by Boltzmann's transport equation. The validity of this equation assumes that (Ferry *et al.*, 2009): (i) the scattering process is local in space and time, (ii) the scattering is weak and the electric field is small, and (iii) the de Broglie wavelength of the electron at the Fermi surface is much smaller than the distance between impurities. The systems amenable to such description are said to be *self averaging*. (In 2D, both σ and G have the same units, $1/\Omega$.)

When the system's size is reduced, we enter the realm of mesoscopic physics. It is instructive to compute the order of magnitude of the number of impurities in a graphene flake with an area of $A = L^2$, and $L = 0.25 \mu\text{m}$ (see Sec. I). Taking $N_i/A = 5 \times 10^{11} \text{ cm}^{-2}$ as a typical impurities' concentration in graphene (see Sec. IV.B for understanding the origin of this number), we obtain $N_i \sim 3 \times 10^2$ impurities. The typical distance between impurities is $d \sim \sqrt{A/N_i} \sim 0.02 \mu\text{m}$; a typical Fermi wave number for the electrons in graphene is $k_F \sim 0.003 \mu\text{m}^{-1}$ (see Sec. IV), from which follows that de Broglie wavelength of the electrons at the Fermi surface is $\lambda_F = 2\pi/k_F \sim 0.02 \mu\text{m}$, making d and λ_F of the same order of magnitude. In this regime, the current becomes non-homogeneous and sensitive to the position of the impurities in the material. Then, the conductance shows fluctuations from sample to sample, and the concept of conductivity loses its meaning. Metallic systems such as graphene are considered highly conducting but disordered metals. The behavior of the electrons becomes sensitive to the metal contacts, surfaces, and interfaces as well and quantum mechanical interference effects become important. Due to these interference effects, the transport properties of mesoscopic systems in the ballistic regime are better assessed by the Landauer's formalism (Ferry *et al.*, 2009).

In calculating the conductance of pristine graphene ribbons, we assume a ribbon of length L_x and width L_y , connected to heavily doped (say, with electrons) graphene leads (see Fig. 10 for the geometry of the device). The doped graphene leads will act as electron reservoirs, and the doping is modeled by gating the leads at a potential V_g .

Since the leads are gated, there is a mismatch between the longitudinal momentum k_x of the electrons in the leads and in the central part of the device, where the undoped graphene ribbon lies; in the device electrons have longitudinal momentum q_x . The momentum k_y is in this case a conserved quantity. The problem is then that of computing the transmission amplitude for an electron coming from the left lead to emerge at the right one. The energy of the electrons at the right and left leads is given by $E = -eV_g \pm v_F \sqrt{k_x^2 + k_y^2}$; in the central region the energy is given by $E = \pm v_F \sqrt{q_x^2 + k_y^2}$. We further impose periodic boundary conditions along the transverse direction, which gives $k_y = 2\pi n/L_y$ with $n = 0, \pm 1, \pm 2, \dots$. Since we are interested in graphene's transport properties at the Dirac point, we have to consider the case of zero energy. For this energy, the solution of $\sqrt{q_x^2 + k_y^2} = 0$ gives $q_x = ik_y$ and therefore the propagation of the electrons in the central region proceeds by means of evanescent waves.

The scattering problem requires writing the wave function on the left and right leads, and on the central region

(Katsnelson, 2006; Tworzydło *et al.*, 2006). In the left lead, the wave function, up to a multiplicative factor of e^{iyk_y} , reads

$$\psi_L(\mathbf{r}) = \begin{pmatrix} 1 \\ e^{i\theta(\mathbf{k})} \end{pmatrix} e^{ik_x x} + r_n \begin{pmatrix} 1 \\ -e^{-i\theta(\mathbf{k})} \end{pmatrix} e^{-ik_x x}. \quad (10)$$

In the central region the wave function can be written as

$$\psi_C(\mathbf{r}) = a_n \begin{pmatrix} 0 \\ 1 \end{pmatrix} e^{-k_y x} + b_n \begin{pmatrix} 1 \\ 0 \end{pmatrix} e^{k_y x}. \quad (11)$$

Finally, in the right lead we have

$$\psi_R(\mathbf{r}) = t_n \begin{pmatrix} 1 \\ e^{i\theta(\mathbf{k})} \end{pmatrix} e^{ik_x x}. \quad (12)$$

The calculation of the transmission amounts to imposing the continuity of the wave function at $x = 0$ and $x = L_x$ and determining the transmission amplitude t_n from which the transmission associated to a given transverse mode n is obtained as $T_n = |t_n|^2$ (to each quantized k_y momentum corresponds a n transverse mode). The final result for the total transmission at zero energy is (Katsnelson, 2006; Tworzydło *et al.*, 2006): $T = \sum_n T_n \simeq \sum_n 1/\cosh^2(k_y L_x)$. As stated, the conductance G is expressed in terms of the conductivity σ as $G = 4e^2 T/h = \sigma L_y/L_x$. In the regime $L_y/L_x \gg 1$, corresponding to ballistic transport, we have $T \simeq L_y/(L_x \pi)$, and therefore $\sigma = \sigma_{\min}$, the same value obtained in Eq. (9), due to disorder. We stress that, for graphene ribbons, only in the regime $L_y/L_x \gg 1$ is the conductivity a well defined quantity, since only in this case is this quantity independent off the aspect ratio of the ribbon.

The extension of this type of calculations to finite temperatures is elementary, and it follows from the Landauer's formalism as well. Such theoretical investigations were done and the results seem to be in qualitative agreement with transport measurements made in high-mobility suspended graphene (Müller *et al.*, 2009).

The conductance of ribbons, with aspect ratio $L_y/L_x \gg 1$, was experimentally measured, and the value $\sigma = \sigma_{\min}$ was obtained (Danneau *et al.*, 2008; Miao *et al.*, 2007) in agreement with the previous result. There are, however, difficulties associated with measuring the conductivity of graphene ribbons at the neutrality point (Blake *et al.*, 2009), since inhomogeneous samples tend to overvalue the minimum of conductivity and two-probe measurements are generally expected to undervalue it (Blake *et al.*, 2009). Due to these subtleties, there is some reserve in the community (Blake *et al.*, 2009) regarding the measured conductances (Danneau *et al.*, 2008; Miao *et al.*, 2007).

We note that the above result for σ_{\min} , being equal to that computed in Sec. III.B, has a different physical origin. The result obtained here is only valid in the regime $L_y/L_x \gg 1$, when the system is in the ballistic regime.

However, one must recognize that the presence of the evanescent modes in the above calculation produces a finite density of states at the Dirac point, precisely what happens in the bulk disordered graphene calculation discussed in Sec. III.B. When the calculation just described for graphene in ballistic regime ($L_y \gg L_x$) includes the effect of resonant scatterers, the conductance is corrected by the value $\delta G = 4\sigma_{\min}/\pi$, per resonant scatterer (Titov *et al.*, 2010), that is, we have impurity-assisted tunneling (Titov, 2007).

As a last comment, we note that the important topics of edge disorder (Gallagher *et al.*, 2010; Lewenkopf *et al.*, 2008; Mucciolo *et al.*, 2009) and Coulomb blockade in graphene nanoribbons are not considered in this Colloquium, since they have been considered elsewhere (Dubois *et al.*, 2009). A review on the effect of disorder on the electronic transport in graphene nanoribbons is also available (Mucciolo and Lewenkopf, 2010).

D. Puddles

We now address the fact that the model developed in Sec. III.C for the conductivity of graphene at the Dirac point is somewhat simplistic, since it assumes the possibility to have graphene with exactly zero electronic density at $E = 0$, the neutrality point.

The physics close to the Dirac point is different from that at finite densities (to be discussed in Sec. IV) as suggested by the data shown in Fig. 6. In Sec. IV we show that the electronic density n can in graphene on top of silicon oxide be externally controlled by a gate potential V_g and given by $n \simeq 7.2 \times 10^{10} \times V_g \text{ cm}^{-2}$. According to this equation, the electron density can be tuned all the way down to zero by changing the gate potential. However, in Fig. 6 we show that the absolute value of the electron density never drops below its theoretically predicted value for $V_g = 2 \text{ V}$. This experimental fact hints for different physics close to the Dirac point, where the system shows important charge-density fluctuations caused by the random electrostatic potential due to sub-surface charged impurities. We, however, stress that in suspended annealed graphene the electronic density can be made as low as $\sim 10^8 \text{ cm}^{-2}$, which corresponds to about a single electron present in a micron size device. Additionally, graphene's topography shows corrugations, which are probably due to roughness in the underlying SiO_2 surface and due to intrinsic ripples of the graphene sheet.

As mentioned, the calculations in Secs. III.B and III.C assume as the starting point that graphene is a perfectly flat material, with null electronic density everywhere. However, experiments using a scanning single-electron transistor (Martin *et al.*, 2008) found that the idealized models of Secs. III.B and III.C do not hold. Those investigations (Martin *et al.*, 2008) found undoped graphene

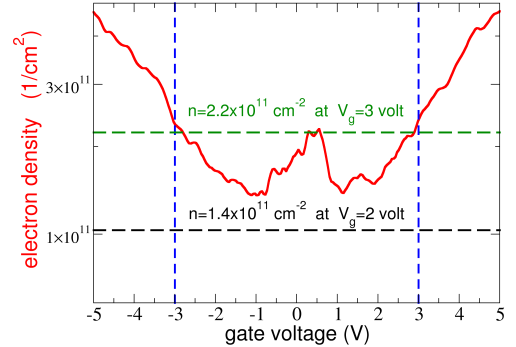


Figure 6 (Color online) Dependence of the absolute value of electron density on the gate voltage V_g . In Sec. IV, we show that the electron density n as function of the gate voltage follows $n = 7.2 \times 10^{10} V_g \text{ cm}^{-2}$. Using this, the electron density for $V_g = 3 \text{ V}$ should be $n \simeq 2.2 \times 10^{11} \text{ cm}^{-2}$ whereas for $V_g = 2 \text{ eV}$ we should have $n \simeq 1.4 \times 10^{11} \text{ cm}^{-2}$. It is clear that for $V_g = 3$ the electronic density is the predicted one; however n never equals its predicted value for $V_g \lesssim 2 \text{ V}$. Note that the vertical scale is logarithmic. (Data from M. Monteverde *et al.* (Monteverde *et al.*, 2010), courtesy of M. Monteverde.)

to be a non-homogeneous system, with electron and hole puddles coexisting, with variations in the electronic density in the range $n \in [-1, 1] \times 10^{11} \text{ cm}^{-2}$, which corresponds to a spatial variation of the surface electrostatic-potential in the range $[-0.25, 0.25] \text{ V}$, with a full width at half maximum of 50 mV. The behavior shown in Fig. 6 is an indirect signature of this experimental fact. The existence of puddles renders the descriptions of Secs. III.B and III.C unsuitable.

Posteriorly, a scanning tunneling microscopy (STM) study (Zhang *et al.*, 2009) was able to provide detailed information on the size and electronic density value of the puddles. This study allowed one to characterize the puddles with electron-density spatial resolution two orders of magnitude higher than previous investigations (Martin *et al.*, 2008). From the results of Sec. II, we can write a relation between the electronic density and the energy as $n = E^2 / (\pi v_F^2 \hbar^2)$. Given the presence of the puddles, the energy becomes function of position, as does the electronic density. We thus have a relation between the electronic density at the Dirac point and the energy, reading

$$n(x, y) = \frac{E_D^2(x, y)}{\pi v_F^2 \hbar^2}. \quad (13)$$

The STM allows the determination of $E_D^2(x, y)$, from which $n(x, y)$ is obtained. These studies revealed that the average lateral dimension of the puddles is of the order of $\sim 20 \text{ nm}$ [a theoretical study (Rossi and Das Sarma, 2008) obtained a similar value], and that each of these puddles contains, on average, a charge of 0.3 ± 0.2 elec-

tron. A Kohn-Sham theory of the carrier-density distribution of massless Dirac fermions in the presence of arbitrary external potentials has also predicted the existence of the puddles (Polini *et al.*, 2008). It was experimentally determined that the topographical corrugations in graphene are about an order of magnitude smaller than the puddles' size, and therefore cannot justify their origin. Indeed, it was established that individual sub-surface charged impurities are responsible for the formation of the puddles. It was estimated that the charge fluctuations associated with a single of those impurities is of the order of 0.07 ± 0.03 electron. There is, therefore, a consensus that the physics of the puddles is due to charged scatterers. The origin of such charged scatterers is likely to be due to chemical species physisorbed onto graphene, which have been trapped in between the substrate and the graphene sheet during fabrication process of the device.

From a theoretical point of view, graphene in the puddles regime can be thought as a random resistor network (Cheianov *et al.*, 2007). Since Klein tunneling (Beenakker, 2008) is exponentially suppressed if the barriers are not perfect potential steps (Cheianov and Fal'ko, 2006), a large electronic transmission will not occur, except for perfectly normal incidence [things are markedly different for magnetic barriers as opposed to electrostatic ones (Martino *et al.*, 2007)]; the essential physics relating the smoothness of potential barriers to the suppression of Klein tunneling was studied in the early days of relativistic quantum mechanics, following a suggestion by Bohr (Christillin and d'Emilio, 2007; Sauter, 1931). The validity of the random resistor model depends on the assumption that transport is incoherent at scales larger than the puddle sizes. Due to Klein tunneling, massless Dirac electrons cannot also localize (Anderson localization) (Cheianov and Fal'ko, 2006; Katsnelson *et al.*, 2006; Lewenkopf *et al.*, 2008; Mucciolo *et al.*, 2009) under the effect of the random electrostatic potential (long-range scatterers) creating the puddles; this accounts for the finite conductivity of graphene at the Dirac point. As discussed in Sec. V.B, long range scatterers preclude the possibility of weak localization effects, and since the electrostatic potential variations can be attributed to charged impurities, the description of transport at the Dirac point based on such type of scatterers seems to be the correct approach (Adam *et al.*, 2007).

We note that intra-cone backscattering (see Sec. V.B) has been shown to be present in graphene (Zhang *et al.*, 2009), which in view of Klein tunneling is a rather interesting experimental fact. Finally, when strong intervalley scattering is present, electrons in graphene can localize.

IV. THE TRANSPORT PROPERTIES OF GRAPHENE AT FINITE ELECTRONIC DENSITY

In the previous section we discussed STM experiments supporting the theory (Polini *et al.*, 2008; Rossi and Das Sarma, 2008) that charge scatterers dominate the electronic transport of neutral graphene. In the ensuing sections, we discuss transport in doped graphene, analyzing the role that resonant and charged scatterers play in this regime.

A. The dependence of the conductivity on the gate voltage

We now discuss the dependence of the conductivity of graphene on the gate voltage, considering two different types of scatterers: resonant scatterers (strong short-range scatterers) and charged impurities. We shall not discuss here scattering from random strain (Katsnelson and Geim, 2008), which we defer to Sec. IV.D.

The electronic density in graphene can be controlled by the back-gate of a device engineered as a plane capacitor – a field effect transistor, made of silicon oxide (relative permittivity $\epsilon = 3.9$), with a thickness b of ~ 300 nm. According to elementary electrostatics, the electric field in the dielectric is given by $E_{\text{cap}} = en/(\epsilon_0\epsilon)$, with n the surface electronic density of graphene, which acts as one plate of the capacitor. The gate potential is related to the electric field by $E_{\text{cap}} = V_g/b$, and so the density of induced charge is $n = \epsilon_0\epsilon V_g/(eb)$. Inserting the numerical values of ϵ and b , we obtain $n = \alpha V_g$, with $\alpha \simeq 7.2 \times 10^{10} \text{ V}^{-1} \cdot \text{cm}^{-2}$. The Fermi momentum k_F is obtained via $k_F = \sqrt{\alpha\pi V_g}$, a result derived by counting the states in momentum space up to k_F .

Ever since the original paper on graphene (Novoselov *et al.*, 2004), demonstrating the ambipolar field effect, it became clear that the conductivity of graphene depends on the gate voltage in some circumstances roughly as $\sigma(\epsilon_F) \propto V_g$; this is shown in Fig. 8, after some replotting of the data (solid curve on the right panel). Experiments also show conductivities presenting a sub-linear behavior; see Figs. 7 (solid curves) and Fig. 8 (dashed curve on the right panel). Mobilities, a measure of the quality of the electronic transport (see caption of Fig. 5 for the definition of the mobility μ), as high as $\mu \sim 1 \times 10^7 \text{ cm}^2 \cdot \text{V}^{-1} \cdot \text{s}^{-1}$, have been indirectly measured by Landau level spectroscopy (Li and Andrei, 2007; Li *et al.*, 2009) of graphene flakes on top of graphite (Neugebauer *et al.*, 2009), raising the question of how perfect can graphene be (Neugebauer *et al.*, 2009). Ultimately, the answer requires the identification of the limiting sources of electronic scattering in graphene (among those listed in Sec. III.A).

An approach combining Fermi's golden rule, Boltzmann equation, the Coulomb potential created by screened charged impurities, and a random phase approx-

imation calculation of the dielectric function of graphene (Shung, 1986; Wunsch *et al.*, 2006) gave a first good account of the observed $\sigma(\epsilon_F) \propto V_g$ behavior for graphene's conductivity (Adam *et al.*, 2008, 2007; Hwang and Das Sarma, 2008). When graphene was doped with potassium (Chen *et al.*, 2008), the measured conductivity agreed with the theory (Adam *et al.*, 2007), as expected. [We note that the conductivity of graphene covered by metal clusters it is still far from being fully understood (Pi *et al.*, 2009).]

Using the same approach for a delta-function potential (Adam *et al.*, 2008, 2007; Hwang and Das Sarma, 2008), the prototype of a short range scatterer, the computed conductivity is a constant number, independent of the gate voltage and of the dielectric constant of the medium. In what follows, we argue that this result is inconsistent. We note that an attempt to solve the Lippmann-Schwinger equation for a delta-function potential showed that this problem is ill defined (regularization of the problem is required in order to have a well-defined problem; as usual, this procedure introduces a length scale. This length scale is interpreted as the range of the short-range potential), and therefore the first Born approximation cannot be trusted. Indeed, exact numerical calculations show that the first Born approximation is inadequate to describe the role of strong short-range scatterers in graphene (Kłos and Zozoulenko, 2010). At the same time, a numerical calculation using the Kubo-Greenwood formalism (Nomura and MacDonald, 2007) showed that $\sigma(\epsilon_F) \propto V_g$ for charged impurities (the level broadening due to scattering was however introduced by hand). The same work (Nomura and MacDonald, 2007) also showed that short-range impurities do produce a conductivity that depends on the gate voltage, but in a sub-linear manner. Also, previous calculations of $\sigma(\epsilon_F)$ based on the SCBA showed that strong short-range scatterers, described by delta-function potentials, do give rise to a gate-voltage-dependent conductivity (Peres *et al.*, 2006; Shon and Ando, 1998), a result embodied in Eq. (9). A similar conclusion was obtained from a semi-classical approach taking into account the chiral nature of massless Dirac fermions (Trushin and Schliemann, 2008).

The two different results – those based on Fermi's golden rule, as opposed to those obtained from the SCBA, for strong short-range potentials – are easily understood: the SCBA is a non-perturbative method, suitable for strong short-range potentials, which takes into account the large deviation of the wave function, within the potential range, from the usual plane wave used in the first Born approximation, as pointed out by Peierls (Peierls, 1979): indeed, the first Born approximation produces a large scattering cross section, whereas the exact calculation gives a small value. Since the conductivity depends on the scattering (transport) cross section, an incorrect determination of it will give, at least, an incorrect value for the impurity concentration in the material.

Unfortunately, the reliance on the result based on Fermi's golden rule is widespread in the community and is being used to fit the experimental data (Hong *et al.*, 2009), at the same time that the resonant scattering mechanism points toward the presence in the material of strong localized potentials (see Sec.III.A).

If it is certain that some amount of charged impurities is present at the silicon oxide-graphene interface (responsible for the electron and holes puddles), it is no less true that experiments do not rule out other sources of scattering. Indeed, recent experiments showed that both adsorbed hydrogen and vacancies led to conductivity curves indistinguishable in form from those of pristine graphene (Chen *et al.*, 2009; Elias *et al.*, 2009). The presence of these short-range scatterers – vacancies and hydrogen – is signaled by a significant Raman D -band intensity (Chen *et al.*, 2009), since they couple electron states from the \mathbf{K} and \mathbf{K}' valleys (see Sec. V.B). By the same token, the presence in pristine graphene of such D -band would be the signature of the presence of short-range scatterers in the material. Detailed Raman investigations in pristine graphene have been carried out (Ni *et al.*, 2010), showing that, indeed, a small D -peak is present in the Raman spectrum of the pristine material. Subsequent transport experiments (Ni *et al.*, 2010) support strong short-range scatterers as the limiting source of scattering in graphene.

An experiment especially designed to address the importance of charged impurities used devices with dielectrics having high permittivity constants (Ponomarenko *et al.*, 2009). These experiments did not exclude completely the contribution of this type of impurities, but did challenge the idea that charged impurities are the main source of scattering in graphene.

On the other hand, in another set of experiments, an apparently similar investigation was done, but with ice layers on top of graphene and reaching a different conclusion. It was argued that the results were consistent with charge scattering (Jang *et al.*, 2008). There is, however, at least one difficulty with the arguments developed in that work: the number of ice atomic layers was at the most six and therefore can hardly be considered an infinite dielectric made of ice; the lines of the electric field are essentially in the vacuum (Silvester and Ferrari, 1996; Sometani, 2000).

A number of questions can still be asked (Monteverde *et al.*, 2010; Ponomarenko *et al.*, 2009; Schedin *et al.*, 2007):

1. In a study of graphene's sensitivity to gases (Schedin *et al.*, 2007) (NO_2 , H_2O , and iodine acting as acceptors, whereas NH_3 , CO , and ethanol acting as donors), chemically-induced charge-carriers concentrations as large as $50 \times 10^{10} \text{ cm}^{-2}$ were achieved. The induced chemical doping shifted only the neutrality point of the conductivity curves, without any significant changes either in the shape

of those curves or in the mobility of the devices; the estimated concentrations of added charged scattering centers was high as 10^{12} cm^{-2} (Schedin *et al.*, 2007). Why is it that no appreciable changes in the mobility were measured in these experiments? [One possible way out can be envisioned: the chemical dopants may cluster, and this would reduce the effectiveness of their scattering effect (Katsnelson *et al.*, 2009).] We also note that the definition of the mobility used in the analysis of the data (Schedin *et al.*, 2007) has been criticized in the literature (Hwang and Das Sarma, 2007).

2. In a study designed to test the prediction (Hwang and Das Sarma, 2008) of the charge scattering model for the ratio of the transport scattering time τ and the elastic scattering time τ_e for both monolayer and bilayer graphene, the experiments found disagreement between the predicted behavior and the measured data, for both graphene systems. The measured deviations were found to be stronger for bilayer graphene (Monteverde *et al.*, 2010). Further, it was found that the measured data agree with the resonant scattering mechanism. How to reconcile this set of measurements with models explaining the mobility of both monolayer and bilayer graphene based on the charge scattering mechanism (Zhu *et al.*, 2009)? [We mention that Monteverde's *et al.* results must be confronted with those of a similar experiment (Hong *et al.*, 2009), reaching different conclusions.]
3. Since screening is strongly dependent on the value of the permittivity ϵ of the surrounding medium, why is the mobility almost insensitive to changes of this parameter? For example, ϵ for ethanol changes from 25 to 55 as the temperature drops from 300 K down to ~ 160 K, but an experiment done in ethanol showed no variation of graphene's mobility. We, however, note that in some experiments (Ponomarenko *et al.*, 2009) a certain amount of variation in the mobility was measured in some devices upon changing the dielectric constant. This result does show that charged impurities play some role as scattering centers but apparently not the limiting one.

The answers to the above questions remain debatable to some extent. The clarification of some of these issues could be taken to an ultimate test using a solid dielectric with a high relative permittivity. It just happens that strontium titanate (SrTiO_3) has a relative permittivity of about 10,000 below $T = 50$ K, which suddenly drops to 300 when the temperature rises above 50 K. A device using such a dielectric would produce a dramatic change of the mobility upon a drop in temperature below 50 K.

If we now refocus our attention on the role of strong short range scatterers, we recall that both the linear

and sub-linear behaviors can be accommodated within a model based on what is now called *resonant scatterers dominated conductivity*, giving rise to mid-gap states (Basko, 2008; Robinson *et al.*, 2008; Stauber *et al.*, 2007; Wehling *et al.*, 2009, 2010), plus the additional effect of charged impurities, which, however, do not play the central role. On the other hand, the simplest model based on short range scatterers, in which the effect of charged impurities is ignored, does not account for the observed dependence of the mobility on the dielectric constant of the device, which has been shown experimentally to be present to some extent (Ponomarenko *et al.*, 2009). In Sec. IV.B we present the main results of such a simple model, and in Sec. IV.C we include the role of charged impurities, and an improved model taking into account both types of scatterers is given. This latter model is a simple combination of results already available in the literature, albeit presented with a different emphasis.

We stress that from the analysis of the SCBA results we see that features showing at energies close to the Dirac point are all proportional to $\sqrt{n_i}$ (recall that n_i is the density of impurities per unit cell), as shown in Fig. 4. This introduces an energy scale $\epsilon_{\min} \lesssim \hbar v_F \sqrt{n_i} / a_0$, below which electron scattering based on plane waves breaks down, meaning that close to the Dirac point the results of Secs. IV.B and IV.C are expected not to hold.

Both models based on mid-gap states or on charged impurities, presented below, fail to give a satisfactory account of the physics close to the Dirac point, since they are based on the scattering of plane waves.

Finally, in suspended graphene (Bolotin *et al.*, 2008a,b; Du *et al.*, 2008), where the material is hanging over a trench, mid-gap states are expected to survive, since some fraction of the corresponding scatterers will still be present, whereas charged impurities are expected to be absent. In the suspended situation, the mobility of the material will be limited only by resonant scatterers plus ripples induced by strain due to the electric field created by the gate (Bao *et al.*, 2009; Fogler *et al.*, 2008).

B. Partial-wave description of resonant scatterers

We assume the presence of short-range scatterers, which we model here as disks of radius R , and whose origin was discussed in Sec. III.B. The effect of the scatterers is such that the electron wave function is zero for $r < R$. The sizes of these disks are of the order of the size of the primitive lattice vectors. The circular shape takes the isotropy of the scattering process into account, and the boundary condition allows a simple analytical solution. A vacancy is one of the possible physical realizations of the model just introduced.

The Dirac Hamiltonian (3) in polar coordinates r and φ reads (Hentschel and Guinea, 2007; Peres *et al.*, 2009a;

Recher *et al.*, 2007)

$$H_{\mathbf{K}} = -iv_F \hbar \begin{pmatrix} 0 & L_- \\ L_+ & 0 \end{pmatrix}, \quad (14)$$

with $L_{\pm} = e^{\pm i\varphi}(\partial/\partial r \pm ir^{-1}\partial/\partial\varphi)$. A particular solution of Eq. (14) with eigenvalue $v_F \hbar k$ has the form $\psi_m(rk) \propto (J_m(kr)e^{-im\varphi}, -iJ_{m+1}(kr)e^{-i(m+1)\varphi})^\dagger$, where $J_m(z)$ is the regular Bessel function of first kind and integer order m . This solution corresponds to a partial wave in the angular momentum representation of the plane wave. In the presence of the potential created by the disk we write the trial wave function as

$$\psi(rk) = A \begin{pmatrix} J_m(kr)e^{im\varphi} \\ iJ_{m+1}(kr)e^{i(m+1)\varphi} \end{pmatrix} + B \begin{pmatrix} Y_m(kr)e^{im\varphi} \\ iY_{m+1}(kr)e^{i(m+1)\varphi} \end{pmatrix}, \quad (15)$$

where $Y_m(z)$ is the irregular Bessel function of first kind and integer order m . We consider that at $r = R$ the wave function satisfies the zig-zag boundary conditions (Akhmerov and Beenakker, 2008; Dominguez-Adamé, 1990), $\psi_{1,m}(kR)/\psi_{2,m}(kR) = 0$, where $\psi_{i,m}(kr)$, with $i = 1, 2$, is the i -component of the Dirac spinor. This boundary condition makes sense since, as discussed in Sec. III.A, a resonant scatterer can effectively behave as a vacancy; in turn, a vacancy is a three-site zig-zag edge. This boundary condition also represents the limiting case where the electronic probability flux is zero through the region where the potential is finite. The phase shift $\delta_m(kR)$ of the m partial wave is given by (Basko, 2008; Hentschel and Guinea, 2007; Katsnelson and Novoselov, 2007; Stauber *et al.*, 2007; Wehling *et al.*, 2009)

$$\tan \delta_m(kR) = \frac{J_m(kR)}{Y_m(kR)}. \quad (16)$$

The relative importance of the several phase-shifts to the transport scattering cross section $\sigma_T(kR)$ depends on the value of $k_F R$. In 2D, the differential cross section, $\sigma(\varphi)$, reads $\sigma(\varphi) = |f(\varphi)|^2$, with $f(\varphi)$ given by

$$f(\varphi) = \sqrt{\frac{2i}{\pi k}} \sum_{m=-\infty}^{\infty} e^{i\varphi m} e^{i\delta_m(k)} \sin[\delta_m(k)]. \quad (17)$$

When $k_F R < 1$, the s -wave phase shift $\delta_0(k_F R)$ is the dominant contribution. Making use of the relation $1/\tau(k) = n_i v_F \sigma_T(kR)/A_c$ (Ziman, 1979), where $\tau(k)$ is the transport relaxation time (see also Sec. V.A), and since the total transport cross section $\sigma_T(kR)$ is obtained from

$$\sigma_T(kR) = \int_0^{2\pi} d\varphi \sigma(\varphi) (1 - \cos \varphi), \quad (18)$$

the conductivity $\sigma(k_F)$ is given by (both spin and valley degeneracies included)

$$\sigma(k_F) = e^2 v_F^2 \frac{\tau(k)}{A_c} \rho(\epsilon_F) = e^2 v_F \frac{\rho(\epsilon_F)}{n_i \sigma_T(k_F R)}, \quad (19)$$

with $\sigma_T(k_F R) = 4 \sin^2 \delta_0(k_F R)/k_F$. Since we assume $k_F R < 1$, we also have $1/\delta_0(k_F R) \simeq 2 \ln(k_F R)/\pi$, and the final result for the dc-conductivity is then

$$\sigma(k_F) = g_0 \frac{3\sqrt{3}}{4\pi} \frac{a_0^2 \alpha V_g}{n_i} \ln^2(\sqrt{\alpha\pi V_g} R). \quad (20)$$

The result (20) for the conductivity holds as long as the Fermi momentum is larger than $k_F \gtrsim \epsilon_{\min}/(\hbar v_F)$ (recall previous discussion). The conclusion is that resonant scatterers (strong short-range impurities), giving rise to mid-gap states, give a conductivity that is gate voltage dependent, with sub-linear or quasi-linear dependence on V_g , depending on the size of the scattering disk R . Furthermore, the conductivity (20) is not independent of V_g even if we take R to be of the order of the carbon-carbon distance, a_0 .

In the first experimental study of the conductivity of suspended graphene (Du *et al.*, 2008), it was shown that this quantity is well described by fitting it to a model of mid-gap scattering states, that is Eq. (20).

In Fig. 7, we fit the conductivity data of suspended and non-suspended graphene using Eq. (20). In all cases a good fit is obtained, using impurity densities ranging from $1.3 \times 10^{11} \text{ cm}^{-2}$ for non-suspended samples down to $0.7 \times 10^{10} \text{ cm}^{-2}$ for suspended ones. We note that for the devices termed *K17* and *K12* in Fig. 7 the n_i values used are $n_i \simeq 0.8 \times 10^{11} \text{ cm}^{-2}$ and $n_i \simeq 1.3 \times 10^{11} \text{ cm}^{-2}$, respectively. The attempt to fit the same data with charged scatterers (Adam *et al.*, 2008, 2007; Hwang and Das Sarma, 2008) gave concentrations of $2.2 \times 10^{11} \text{ cm}^{-2}$ and $4.0 \times 10^{11} \text{ cm}^{-2}$ for *K17* and *K12*, respectively. The two set of numbers for n_i have the same order of magnitude, but Eq. (20) gives a better fit to the data, except for the measurements shown in the top left panel of Fig. 7. For this particular device, made of suspended graphene, the maximum of the measured conductivity is about two times smaller than that measured in the other suspended device, whose data are shown in the top right panel of Fig. 7, suggesting that additional sources of disorder may have been introduced during the fabrication process. We stress that the fits done in Fig. 7, use the density of impurities as the only fitting parameter since R has to be of the order of a_0 (Wehling *et al.*, 2010); changes of order one in the value of R give small changes for the impurity concentration.

Some phenomenological approaches (Morozov *et al.*, 2008) have tried to reconcile the measured sub-linear behavior of the conductivity of graphene with the linear behavior (upon V_g) predicted by the charge scatterers model. In the case of the data given in the right

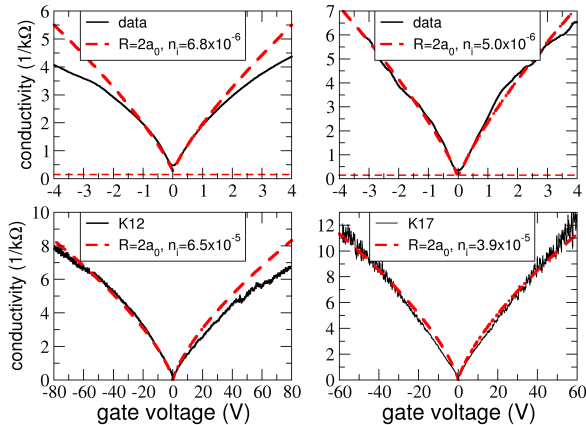


Figure 7 (Color online) The conductivity of suspended and non-suspended graphene as function of the gate voltage. **Top panels:** Conductivity of suspended graphene from two different devices, after current annealing ($\ell \sim 1 \mu\text{m}$). The **top left** panel corresponds to a device with $\mu \sim 170,000 \text{ cm}^2 \cdot \text{V}^{-1} \cdot \text{s}^{-1}$, at electronic density of $n = 2 \times 10^{11} \text{ cm}^{-2}$ [data from K. I. Bolotin *et al.* (Bolotin *et al.*, 2008a), courtesy of K. I. Bolotin]. The **top right** panel corresponds to a device with $\mu \sim 200,000 \text{ cm}^2 \cdot \text{V}^{-1} \cdot \text{s}^{-1}$, at electronic density of $n = 2 \times 10^{11} \text{ cm}^{-2}$ [data from K. I. Bolotin *et al.* (Bolotin *et al.*, 2008b), courtesy of K. I. Bolotin]. **Bottom panels:** Conductivity of graphene on top of silicon oxide, corresponding to devices with $\mu \sim 10,000 \text{ cm}^2 \cdot \text{V}^{-1} \cdot \text{s}^{-1}$ (Data from Y.-W. Tan *et al.* (Tan *et al.*, 2007), courtesy of P. Kim). In all panels the fits use the model developed in Sec. (IV.B), with n_i as the only fitting parameter; R has to be of the order of a_0 (Wehling *et al.*, 2010). In the legends, the concentration of impurities is per unit cell.

panel of Fig. 7, a sub-linear behavior of the conductivity upon V_g (for graphene on top of SiO_2) is evident. A linear behavior could be recovered by defining the measured resistivity ρ_{measured} as a sum of two terms $\rho_{\text{measured}} \equiv \rho_g + \rho_S$, where ρ_S is a fitting parameter. The conductivity $\sigma_{\text{sub}} = 1/\rho_{\text{measured}}$ is sub-linear in V_g , whereas the conductivity $\sigma_{\text{lin}} = 1/(\rho_{\text{measured}} - \rho_S)$ shows linear behavior. The fitting parameter ρ_S was assumed to be independent of V_g , and was attributed to short-range scatterers. The discussion presented above for strong short range scatterers showed that this type of disorder does produce sub-linear behavior of the conductivity upon V_g , even in the case $R \sim a_0$, with the same order of magnitude for impurity concentration as those proposed by the charge scattering mechanism (Adam *et al.*, 2008, 2007; Hwang and Das Sarma, 2008). It is obvious then that, using the curves calculated with the mid-gap state mechanism, it is still possible to obtain a linear dependence of the conductivity on V_g by assuming a ρ_S fitting parameter as done in the phenomenological approach (Morozov *et al.*, 2008). From the discussion in

this section it is fair to say that the origin of ρ_S still needs clarification. Moreover, we can even ask the question whether the parameter ρ_S is really needed for the interpretation of the data.

Finally, we note that in our calculation we have not included the effect of inter-valley scattering, which is known to be present when the scatterers are short-range. If that effect is included, a contribution to the conductivity of the form given by Eq. (20) is found, albeit with a different numerical prefactor (Ostrovsky *et al.*, 2006).

C. Partial-wave description of Coulomb scatterers

We now derive the contribution to the conductivity of graphene due to Coulomb scatterers. We can think of three alternative scenarios for the origin of Coulomb scatterers: either they exist independently of the resonant scatterers, or the latter can themselves be charged, carrying a fraction of the unit charge, or both cases can coexist. Experiments aiming at studying in detail the Raman D peak of pristine graphene, can also shed light on this aspect, by studying suspended pristine graphene before and after annealing.

The solution of the Dirac equation in 2D for the Coulomb potential was obtained more than ten years ago (Lin, 1999) for the sub-critical regime (see below), and rediscovered in the context of graphene by different groups (Novikov, 2007a,b; Pereira *et al.*, 2007; Shytov *et al.*, 2007), who also solved the case of the super-critical regime.

It was known for some time (Lin, 1997) that the Coulomb problem in the 2D Schrödinger equation provides a total cross section which does not coincide with the first Born approximation. The same happens with the 2D Dirac equation (Lin, 1999; Novikov, 2007a; Pereira *et al.*, 2007; Shytov *et al.*, 2007). The discussion given above, restrains us from accepting results based on the first Born approximation without a critical analysis.

For the Coulomb problem, the Hamiltonian has the form $H = H_{\mathbf{K}} + \mathbf{I}Z e^2 / (4\pi\epsilon_0 r)$ (\mathbf{I} a 2×2 identity matrix) and the solution is sought in the form

$$\psi_j(\mathbf{r}) = \frac{1}{\sqrt{r}} \begin{pmatrix} f_j(rk) e^{i\varphi(j-1/2)} \\ \pm i g_j(rk) e^{i\varphi(j+1/2)} \end{pmatrix}, \quad (21)$$

with j a half-integer number. When the trial wave function (21) is inserted into the Dirac equation we get

$$\begin{bmatrix} \epsilon + g/r & -\partial_r - j/r \\ \partial_r - j/r & \epsilon + g/r \end{bmatrix} \begin{bmatrix} f_j \\ \pm i g_j \end{bmatrix} = 0, \quad (22)$$

where $j = m - 1/2$, $\epsilon = E/(v_F \hbar)$, E is the energy, $g = Z\alpha_g$, and $\alpha_g = e^2/(4\pi\epsilon_0 v_F \hbar) \simeq 2.2$ is graphene's fine structure constant. The solution to Eq. (22) has been obtained by several, and the central quantity is the phase

shift of the j partial wave, as in the case of Sec. IV.B. For this problem the phase shifts read

$$e^{2i\delta_j(g)} = \frac{j\Gamma(s-ig)}{\Gamma(s+1+ig)} e^{i\pi(j-s)}, \quad (23)$$

with the property $\delta_j(g) = \delta_{-j}(g)$, $s = \sqrt{j^2 - g^2}$, and $\Gamma(x)$ the usual gamma function; the sub-critical regime is defined by the condition $g < 1/2$. Contrary to the short-range scatterer problem, solved in Sec. IV.B, the phase shifts (23) do not depend on the energy of the incoming particle, but they do depend on the sign of the Coulomb potential and on which type of particle, an electron or a hole, is being scattered. The independence of $\delta_j(g)$ on the energy is simple to understand from a straightforward argument based on dimensional analysis: on the one hand, the Coulomb potential has no intrinsic length scale, and on the other hand, the particle's mass is null. These two facts show that the problem as a whole has no intrinsic length scale (some sort of *Bohr's radius*, as in the non-relativistic theory of the hydrogen atom) and therefore dimensionless numbers involving the momentum k cannot be formed, leading to the conclusion that the dimension of the cross section (dimension of length, in 2D) can only come from the momentum itself. That is, we are then bound to have $\sigma_T(k) \propto 1/k$, which gives the linear dependence on the gate voltage. The electron-hole asymmetry of the cross section can partially account for the measured asymmetry of the conductivity curves. Another source of electron-hole asymmetry of the conductivity is originated in the metal contacts of the transistor (Huard *et al.*, 2008).

The above solution assumes that graphene is floating in vacuum. In a real experiment, graphene is on top of a dielectric, SiO₂ being the most common. Other dielectrics have also been used (Ponomarenko *et al.*, 2009). In these experimental conditions, the value of g is different from that given above.

In the case $Z = 1$ and for graphene on top of a dielectric, a charge e in between the dielectric (with relative permittivity ϵ_d) and graphene, behaves effectively as a charge with a value (Landau *et al.*, 1984; Slater and Frank, 1969) of $e_r = 2e/(1 + \epsilon_d)$. Additionally, the relative permittivity of graphene due to electron-electron interactions is renormalized to $\epsilon_r = 1 + 2\pi\alpha_g/[2(1 + \epsilon_d)]$ (Adam *et al.*, 2007; González *et al.*, 1999; Shung, 1986). These two effects combined give an effective fine structure constant for graphene of

$$\alpha_g^{\text{eff}} = \frac{\alpha_g}{\epsilon_r} \frac{2}{1 + \epsilon_d}. \quad (24)$$

Using the same procedure of Sec. IV.B, the conductivity of graphene due to Coulomb scatterers reads

$$\sigma = e^2 v_F \frac{k_F \rho(\epsilon_F)}{2n_i \Lambda(g)} = g_0 \frac{3\sqrt{3}a_0^2}{8n_i \Lambda(g)} \pi \alpha V_g, \quad (25)$$

Dielectric	ϵ_d	α_g^{eff}	$\Lambda(g)$	$\Lambda(-g)$
H ₂ O	80	0.05	0.013	0.012
Ethanol (160 K)	55	0.07	0.027	0.022
Ethanol (300 K)	25	0.13	0.10	0.07
HfO ₂	25	0.13	0.10	0.07
SiO ₂	4	0.37	1.20	0.46

Table I Dependence of $\Lambda(g)$ on the type of dielectric for both electrons, $g > 0$, and holes, $g < 0$. The impurities are assumed to have valence $Z = -e$. For ethanol, the dielectric function depends on temperature, as indicated between braces. Since graphene is in the ultra-relativistic limit, the value for $\Lambda(g)$ cannot be obtained from adding only few partial waves.

where $\Lambda(g) = \sum_{m=-\infty}^{\infty} \sin^2(\delta_{m+1/2} - \delta_{m-1/2})$. It is worth stressing that $\Lambda(g)$ is different for particles, $g > 0$, and holes, $g < 0$, a behavior not captured by the first Born approximation (Adam *et al.*, 2007). In Table I we give the numerical values for the quantity $\Lambda(g)$, considering graphene on top of or submerged in different dielectrics.

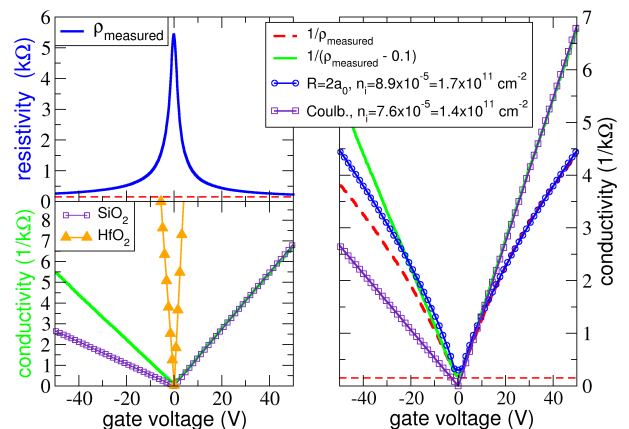


Figure 8 (Color online) Resistivity and conductivity of graphene on top of silicon oxide. **Top left panel:** Raw data of a measurement of the resistivity, ρ_{measured} , of an exfoliated graphene sheet [data from S. V. Morozov *et al.* (Morozov *et al.*, 2008)]. **Right panel:** Fit of the conductivity using Eq. (20) for the case where $\sigma_{\text{sub}} = 1/\rho_{\text{measured}}$, and using Eq. (25) for the case where $\sigma_{\text{lin}} = 1/(\rho_{\text{measured}} - \rho_S)$, with $\rho_S = 100 \Omega$ [the value of $\rho_S = 100 \Omega$ is that used by S. V. Morozov *et al.* (Morozov *et al.*, 2008)]. **Bottom left panel:** Data $\sigma_{\text{lin}} = 1/(\rho_{\text{measured}} - \rho_S)$ fitted with the conductivity formula given by Eq. (25) (squares). For comparison, we give the theoretical conductivity curve (triangles) considering that the experiment had been done using HfO₂ as a dielectric. This allows one to compare the modification of the numerical values of σ due to a substrate change. (Data from S. V. Morozov *et al.* (Morozov *et al.*, 2008), courtesy of A. K. Geim.)

We have now developed all the tools needed to perform the analysis of the data of Fig. 8. We start by fitting the data using the two models presented above separately, that is Eqs. (20) and (25). We must stress that each of these two models have only one fitting parameter: the concentration of impurities (in the model for resonant scattering, the parameter R is fixed by the size of the primitive cell). In the right panel of Fig. 8 we plot the data $\sigma_{\text{sub}} = 1/\rho_{\text{measured}}$ and $\sigma_{\text{lin}} = 1/(\rho_{\text{measured}} - \rho_S)$ using the raw data ρ_{measured} (given in the left top panel of the same figure). In the case of σ_{sub} , the data can be fitted using Eq. (20) for mid-gap states. A perfect fit to both negative and positive gate voltages is not possible, since by construction the model developed in Sec. IV.B preserves electron-hole symmetry; an improvement which does not preserve electron-hole symmetry is easy to develop by considering a large finite value (as opposed to an infinite value) for the effective potential g_{eff} as discussed in Sec. III.A (see also (Araújo and Peres, 2006; Stauber *et al.*, 2008a)); we show below that charged scatterers can account for the loss of electron-hole symmetry of the conductivity curves as well.

In the case of the data computed as σ_{lin} we fit the positive gate voltage region with Eq. (25) for charged scatterers. Note that since $\Lambda(g) \neq \Lambda(-g)$ the computed conductivity has no electron-hole symmetry, an effect seen in the experiments (Chen *et al.*, 2008). Nevertheless, although Eq. (25) does break electron-hole symmetry, the magnitude of the computed effect is far too strong, and therefore Eq. (25) is not able to fit the data over the negative and positive range of V_g , by assuming a single concentration of charged scatterers. It is worth noting that the concentration of impurities used to fit σ_{sub} and σ_{lin} is essentially the same for both types of scatterers. In the left bottom panel of Fig. 8 we depict the conductivity values (triangles), had we performed the same experiment using HfO_2 as a dielectric. To understand such a large change, we look at Table I, where we show that $\Lambda(g)$ can be reduced by one order of magnitude (positive g) from SiO_2 to HfO_2 , leading to the large increase in the conductivity shown in Fig. 8.

We now take into account, in a single model, the effect of both strong short-range and charged scatterers. Computing the conductivity as $\sigma_{\text{sub}} = 1/\rho$, such that (Matthiessen's rule)

$$\rho = \frac{1}{\sigma_{\text{short}}} + \frac{1}{\sigma_{\text{Coulomb}}}, \quad (26)$$

and with σ_{short} computed using Eq. (20) and σ_{Coulomb} determined from Eq. (25), we can fit the data of Fig. 8 quite accurately, as shown in Fig. 9. In this figure, the concentration of impurities leading to mid-gap states used in the fit was $n_{\text{short}} = 1.5 \times 10^{11} \text{ cm}^{-2}$ and that for charged scatterers was $n_{\text{Coulomb}} = 2.4 \times 10^{10} \text{ cm}^{-2}$, about seven times smaller than n_{short} (these two concentrations are, essentially, the only two fitting parameters

in the model). The combined contributions from resonant scatterers and charged impurities allow one to fit σ_{sub} over the whole V_g range, using a single value for the impurity concentrations.

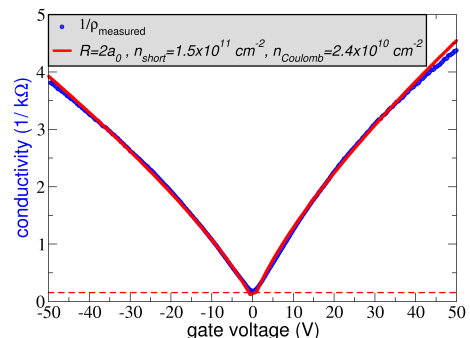


Figure 9 (Color online) The conductivity data $\sigma_{\text{sub}} = 1/\rho_{\text{measured}}$, also plotted in Fig. 8, but fitted using Eq. (26), which combines the effect of resonant and charged scatterers. In the legend, n_{short} and n_{Coulomb} refer to the concentration of resonant and charged scatterers, respectively. The concentration of impurities is the only fitting parameter used in the theory. [Data from S. V. Morozov *et al.* (Morozov *et al.*, 2008), courtesy of A. K. Geim.]

In conclusion, we made a thorough analysis of the role of resonant scatterers (which give rise to mid-gap states) and charge scatterers in the conductivity of graphene, and showed that a coherent picture emerges from a scattering analysis of the transport based on the exact calculation of the phase shifts of scattered chiral Dirac fermions, as opposed to a calculation based on the first Born approximation.

Finally, we note that fine tuning details coming from the dependence of the dielectric constant of graphene on the wave vector (the polarization contributions) were not included in our simple model, except for the important effect of the renormalization of the fine structure constant, which corresponds to the large wave number limit.

Experiments will decide which scenario regarding the limiting source of scattering in graphene actually prevails.

D. Transport across a strained region: A way of generating a transport gap

The main limiting factor of all graphene properties, in what concerns its application to nanoelectronics, is, most likely, the lack of a true band gap, as opposed to the biased graphene bilayer (Castro *et al.*, 2007; McCann, 2006; McCann and Fal'ko, 2006). This fact can, however, be overcome by creating a transport gap.

In nowadays nanotechnology, understanding the effect of strain on the properties of devices is an essential step

toward the improvement of their performance. For example, characterizing how strain can improve the properties of silicon-based devices is a mainstream research topic (Hÿtch *et al.*, 2008). As stated in Sec. III.A, both ripples and wrinkles can act as scattering centers as they effectively create random strain in the material, leading to a modification of the hopping energy t . In what follows, we show that strain in graphene gives rise to a rich structure in the electronic and transport properties of the material.

Being a 2D flexible membrane (Booth *et al.*, 2008; Kim and Castro Neto, 2008), stretching (which in graphene can be as large as 20%, being reversible) and bending graphene in a controlled way is feasible (Ferralis *et al.*, 2008; Kim *et al.*, 2009; Mohiuddin *et al.*, 2009), with consequences to the electronic (Pereira *et al.*, 2009) and transport properties of the material (Fogler *et al.*, 2008; Guinea *et al.*, 2010; Pereira and Castro Neto, 2009; Teague *et al.*, 2009). As we see below, strain can be modeled by a fictitious gauge field (de Juan *et al.*, 2007), which can then act as an effective magnetic field. In some circumstances, it was predicted that this effective magnetic field can have an intensity as high as 10 T (Guinea *et al.*, 2010), leading to a pseudo-magnetic quantum Hall effect. The presence of such an odd quantum Hall effect can, in principle, be experimentally observed using scanning tunneling microscopy, which is a direct measure of the density of states, and, therefore, sensitive to the reorganization of the spectrum due to the presence of the gauge field. Such type of experiments have been performed (Levy *et al.*, 2010) and found strain-induced pseudo-magnetic fields greater than 300 T.

In the case of suspended graphene (Teague *et al.*, 2009) there are two sources of strain. One is induced by the electric field produced by the gate, which pulls the graphene membrane downwards. The solution of the corresponding elasticity problem produces an effective model where the effective vector potential is constant (Fogler *et al.*, 2008; Pereira and Castro Neto, 2009), precisely the model we discuss below. The other source of strain depends on the thermal properties of graphene. Graphene's thermal expansion coefficient is anomalously large and negative (Bao *et al.*, 2009; Faugeras *et al.*, 2010), a feature which can be exploited to induce 1D and 2D ripples (with a periodicity of about 300 nm) possibly leading to novel strain-based engineered graphene devices (Guinea *et al.*, 2010; Pereira and Castro Neto, 2009).

Consider a graphene-based device where the central part of the material, of length L , is a graphene ribbon under strain, with armchair edges oriented along the x -axis, as shown in Fig. 10. The strained part is then connected to two pristine leads. It is well understood that the effect of strain can be included in the Dirac Hamiltonian in the form of a fictitious gauge field (Castro Neto *et al.*, 2009; Guinea *et al.*, 2010). The emergence of the

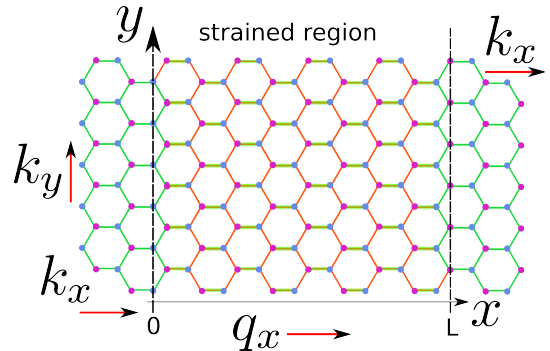


Figure 10 (Color online) Scheme of a device made of strained graphene. The central region is the strained part. In the assumed model, the effect of strain is to modify the hopping connecting a given carbon atom to its three neighbors in such a way that two of the hoppings are equal. Shown is the momentum of the electrons in the leads and in the strained region.

fictitious gauge field is simple to understand. We assume that the hopping along the armchair edge is modified relatively to its pristine value t as $t \rightarrow t + \Delta t$ [a detailed study of how strain changes the value of the hopping was done using *ab initio* methods (Ribeiro *et al.*, 2009)]. This adds a term to the Hamiltonian, Eq. (1), of the form

$$\Delta t \sum_{\mathbf{R}_n} (|A, \mathbf{R}_n\rangle \langle \mathbf{R}_n + a_0 \mathbf{u}_x, B| + H.c.). \quad (27)$$

Passing from the tight-binding description to the continuous model, the contribution from Eq. (27) has a finite value at a given point in space. Since Eq. (27) couples the sub-lattices A and B at the same point in space its contribution to the effective Hamiltonian, Eq. (3), has the simple form (Castro Neto *et al.*, 2009)

$$\mathbf{A}(x, y) \sigma_y = -\theta(x)\theta(L-x) \frac{\Delta t}{ev_F} \mathbf{u}_y \sigma_y, \quad (28)$$

implying that the Dirac Hamiltonian maintains its original form, but with \mathbf{p} replaced $\mathbf{p} \rightarrow (p_x, p_y + e\mathbf{A}_y)$. Clearly, we have a new Hamiltonian where the electrons now couple to a fictitious vector potential \mathbf{A} through the usual minimal coupling of electrons to an electromagnetic field.

The question now is (Pereira and Castro Neto, 2009): How are the transport properties of Dirac electrons changed when transversing a region of strained graphene? As usual, the answer to this question is obtained by computing the transmission of the device by matching the wave functions from the left and right leads to those of the central region, at the positions $x = 0$ and $x = L$. From the matching conditions we compute the total scattering matrix of the system (Nazarov and Blanter, 2009), relating the incoming and outgoing waves. The scattering matrix S is obtained easily from the total transfer

matrix of the structure T_s using the same formalism introduced in Sec. III.C. In this case, the transfer matrix is given by

$$T_s = \frac{1}{D} \begin{bmatrix} u & v \\ v^* & u^* \end{bmatrix} \begin{bmatrix} u^* e^{-iLq_x} & -v e^{-iLq_x} \\ -v^* e^{iLq_x} & u e^{iLq_x} \end{bmatrix}, \quad (29)$$

where $D = 4 \cos \theta \cos \tilde{\theta}$, $u = e^{-i\theta} + e^{i\tilde{\theta}}$, $v = e^{-i\theta} - e^{i\tilde{\theta}}$, $\tan \theta = k_y/k_x$, $\tan \tilde{\theta} = (k_y - \delta)/q_x$, with k_y , k_x , and q_x the transverse momentum, the longitudinal momentum in the leads, and the longitudinal momentum in the device, respectively, and $\delta = \Delta t/(v_F \hbar)$. Finally, the energy in the leads has the form $\epsilon = \sqrt{k_x^2 + k_y^2}$, and in the central region $\epsilon = \sqrt{q_x^2 + (k_y - \delta)^2}$. The last equation shows that the effect of strain is to shift the position of the Dirac point in the Brillouin zone, a crucial effect on the explanation of the following results. Equation (29) was derived for energies in the continuum (no bound states). However, a fundamental property of the scattering matrix (or the T_s matrix for this purpose) is that bound states can also be obtained from the form derived for the scattering states, by looking at the poles of the S matrix. Since the S -matrix is obtained from the inverse of the T_s matrix, its elements contain a factor which is the inverse of the determinant of T_s . Additionally, the S_{11} element of the S -matrix (in this problem the S -matrix is a 2×2 matrix, since we are working on the propagating mode base) gives the amplitude of transmission across the strained region, its value being

$$S_{11} = \frac{4 \cos \tilde{\theta} \cos \theta}{\cos(Lq_x)(|u|^2 - |v|^2) - i \sin(Lq_x)(|u|^2 - |v|^2)}. \quad (30)$$

From Eq. (30), we see that there are energies of perfect transmission, when $Lq_x = n\pi$, with $n = 1, 2, \dots$. On the other hand, considering the case $k_y = 0$, corresponding to normal incidence on the boundary, we obtain for the transmission

$$T = |S_{11}|^2 = \frac{\epsilon^2 - \delta^2}{\epsilon^2 - \delta^2 \cos^2(Lq_x)}, \quad (31)$$

which is a number smaller than one, meaning there is no Klein tunneling through strained graphene. At resonances, $Lq_x = n\pi$, the transmission (31) is one, and for energies in the range $\delta/2 < \epsilon < \delta$, it decreases exponentially with L , since q_x becomes imaginary. In general, for angles (between \mathbf{k} and y -axis) satisfying the condition $\theta_f > \arccos(-1 + \delta/\epsilon)$ the transmission, as computed from Eq. (30), is shown to be strongly suppressed for large L , an effect termed: transport gap formation (Pereira and Castro Neto, 2009). True energy gaps can also be created in graphene by choosing an appropriate geometry of strain (Guinea *et al.*, 2010). The reason behind this transport gap mechanism is easy to understand given the discussion in Sec. II; in the strained region the

electrons' wave function are no longer eigenstates of the helicity operator \hat{h} . Therefore, since the helicity is not a constant of motion in this problem, Klein tunneling is lost and backscattering is allowed.

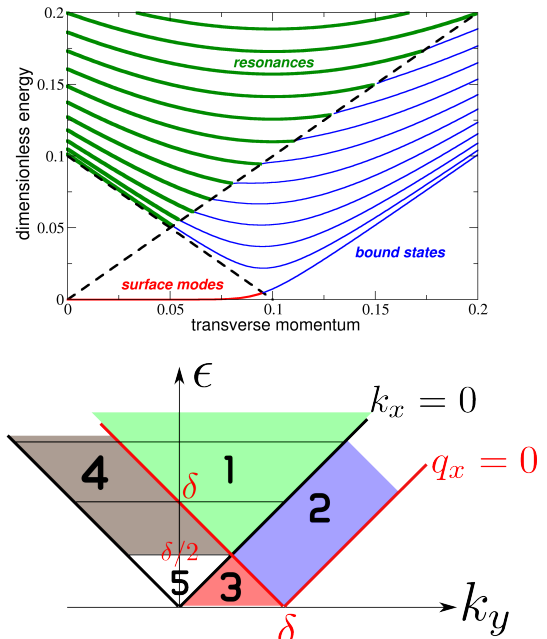


Figure 11 (Color online) Resonances, bound states, and surface states. **Top panel:** The parameters are $L = 100$ and $\delta = 0.1$. In the resonances region, $\epsilon > k_y$, the energy curves corresponds to the momenta $q_x = n\pi/L$. The horizontal axis refer to the transverse momentum k_y , and the vertical one to the dimensionless energy ϵ . **Bottom panel:** Representation in the plane energy versus k_y of the five types of states appearing in this problem. The two Dirac cones, that of the contacts and that of the strained region, are represented for $k_x = 0$ and $q_x = 0$, respectively. The off set of the apex of the two cones is δ . All states with $k_x \neq 0$ and $q_x \neq 0$ lie above the two respective cones.

As mentioned, the denominator of the S_{11} element of the S -matrix is all that it is needed to look for bound states in this system. We can imagine two different types of bound states: those decaying exponentially in the leads, but propagating inside the strained region and those decaying exponentially in the three regions. The latter states are edge states living at the boundaries between the leads and the strained region. Looking only at the poles of S_{11} we can find that both types of bound states exist (Pereira and Castro Neto, 2009). The richness of states in strained graphene is due to the breaking of the chiral symmetry. In Fig. 11 we have represented the energies at which the transmission is unity (called resonances), the energies of the bound states, and the energy of the edge or surface states. The different types of states are a result of the different shifts of the two Dirac cones over the Brillouin zone (Hasegawa *et al.*, 2006; Montam-

baux *et al.*, 2009), induced by the strain and governing the vector potential of Eq. 28; the two apexes are shift by δ due to strain, as seen above.

It was shown (Pereira and Castro Neto, 2009) that in the problem under study there are in total five types of states: (1) scattering states, (2) band states (states localized in the junction along the x -direction) propagating along the y direction (3) localized states at the boundary of the junction, (4) filtered states, that is, scattering states decaying exponentially inside the junction for certain values of the incoming angle θ_f , and (5) and states such that the transmission occurs via evanescent waves for any orientation of the incoming momentum – it is said that all states are filtered. The regions in the energy versus k_y plane where these type of states appear are shown in the bottom panel of Fig. 11.

In conclusion, the example discussed shows that there is *plenty of room at the bottom* of strained graphene for a whole new sub-field of graphene research: that of strain-based transport engineering or straintronics.

V. QUANTUM CORRECTIONS TO THE DRUDE CONDUCTIVITY

Before discussing the quantum corrections to the Drude conductivity, we introduce some key concepts on electronic transport. Consider first the elementary transport theory in a normal metal, where electrons have an effective mass m^* . The velocity of the electrons at the Fermi surface is given by $v_F = \hbar k_F / m^*$, where k_F is the Fermi wave number whose value depends on the density of electrons. Impurities in an otherwise perfect crystal occasionally deflect electrons from free propagation, leading to the appearance of a mean free path l – the mean distance to the next collision. Since the dominant contribution to transport comes from electrons having velocity v_F , we can introduce a phenomenological parameter, the relaxation time τ , defined as $\tau v_F = l$; the elementary theory of transport then shows that the electronic conductivity of the metal reads (Ziman, 1979) (no spin or valley degeneracies included): $\sigma_0 = e^2 n \tau / m^*$. This is a purely classical result, known as Drude's formula, and which assumes that, after each collision, the electron loses memory of its previous linear momentum state. The calculation of τ is usually obtained from Fermi's golden rule. The above description makes sense when $l \gg \lambda_F = 2\pi/k_F$ (Ziman, 1979). If we now repeat the same analysis for graphene, we obtain (Adam *et al.*, 2008, 2007; Basko, 2008; Peres *et al.*, 2007b; Stauber *et al.*, 2007): $\sigma_0 = 2e^2 \tau v_F k_F / h$, where we have now included the contributions of both spin and valley degeneracies.

It is also possible to view the conductivity problem as a random walk. In this case, the conductivity is related to the diffusion constant D through Einstein's relation (Chakravarty and Schmid, 1986): $\sigma_0 = e^2 D \rho(\epsilon_F)$ (here

again no spin or valley degeneracies included), with $\rho(\epsilon_F)$ the density of states per unit area, and the units of D are those of area per time, in any spatial dimension. The diffusion constant, for order of magnitude estimates, can be taken as $D \sim v_F l$.

A. Weak localization in a normal metal

Weak localization is a correction to the classical conductivity of a disordered metal due to quantum interference, and originates in the quantum mechanical superposition principle. Electrons propagating in metals are subjected to a number of scattering mechanisms that give rise to a number of characteristic times.

The relaxation time τ due to elastic collisions with static impurities is assumed to be the smallest scattering time and describes a reversible process. Other scattering mechanisms are irreversible in nature and lead to either the loss of phase coherence or energy relaxation; for instance, those caused by electron-electron and electron-phonon interactions (excluding interactions with magnetic impurities). Contrary to τ , the phase relaxation (or dephasing) time τ_ϕ is temperature dependent and at low temperatures is mainly due to electron-electron interactions. In the presence of a magnetic field, a new time scale τ_B appears, which is of the order of $\tau_B \sim \ell_B^2 / D$, by simple dimensional analysis arguments, and where $\ell_B^2 = \hbar / eB$ is the magnetic length. We now proceed to the discussion of the quantum interference effects using an intuitive approach (Abrikosov, 1988; Beenakker and Houten, 1991), rather than a formal one, as seems appropriate in the context of this Colloquium.

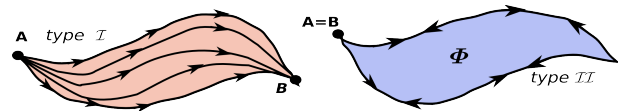


Figure 12 (Color online) Pictorial representation for two types of scattering processes, whose physical interpretation is given in the text. The presence of a finite magnetic field is represented by the flux Φ piercing the area defined by the two time-reversed trajectories.

Imagine an electron traveling from position A to B , as shown in Fig. 12, and we denote by $a_i e^{i\phi_i}$ the probability amplitude for the electron to travel from A to B , along trajectory i . Since there are many indistinguishable trajectories, the total probability of traveling from A to B is

$$P_I(A \rightarrow B) = \left| \sum_i a_i e^{i\phi_i} \right|^2. \quad (32)$$

We now show that quantum interference effects are much more important for what we call trajectories of type II,

in Fig. 12, in which the initial and final points coincide ($A = B$).

For type I trajectories ($A \neq B$), we have

$$P_I(A \rightarrow B) = \sum_i |a_i|^2 + \sum_{i \neq j} a_i a_j e^{-i(\phi_i - \phi_j)}. \quad (33)$$

Since the phases for different trajectories of type I are uncorrelated, we assume that the second term averages to zero, leaving us with the classical result, in which the probability to go from A to B is just the sum of the probabilities over all possible trajectories, that is,

$$P_I(A \rightarrow B) = \sum_i |a_i|^2 = P_I^{(cl)}(A \rightarrow B). \quad (34)$$

However, for trajectories of type II (the same initial and final points), in the presence of time reversal symmetry, the situation is quite different. In fact, time reversed trajectories (going round the loop in clockwise and anti-clockwise fashion), contribute to the sum of Eq. (33) with the same amplitude, in both modulus and *phase*. As a result, in the interference term,

$$\sum_{i \neq j} a_i a_j e^{-i(\phi_i - \phi_j)}, \quad (35)$$

when i and j denote time reversed trajectories, the phases cancel, even before any averaging; this term gives a contribution exactly equal to the first one, since for every trajectory there is a time reversed pair. This then amounts to a probability

$$P_{II}(A \rightarrow A) = 2 \sum_i |a_i|^2 = 2P_I^{(cl)}(A \rightarrow A). \quad (36)$$

This effect of quantum interference therefore enhances the probability of return, relative to the classical result, decreasing diffusion and, therefore, the conductivity (Abrikosov, 1988; Beenakker and Houten, 1991); in other words we have

$$\sigma_{wl} - \sigma_0 < 0, \quad (37)$$

where σ_{wl} stands for the conductivity of the metal considering the enhanced backscattering effect, due to quantum interference. It is the reduction in σ_{wl} relatively to σ_0 that is known as weak localization.

In the presence of a magnetic field \mathbf{B} the relative phase of the electron's wave function, associated with the two time reversed trajectories of type II, has the value $\delta\phi = 4\pi\Phi/\phi_0$ as given by the Aharonov-Bohm effect, where Φ is the magnetic flux piercing the area defined by the closed trajectory. Therefore, applying a magnetic field to the system suppresses the interference effect (because it changes the relative phase to a non-zero value) given by Eq. (36), and the low-temperature conductivity of the

metal increases when the field is turned on; or, in other words, we have

$$\frac{\delta\sigma(B)}{\sigma_{wl}} \equiv \frac{\sigma_{wl}(B) - \sigma_{wl}}{\sigma_{wl}} > 0. \quad (38)$$

Using Eq. (38) we obtain experimental evidence of weak localization effects in the conductivity of a disordered metal.

If the spin-orbit interaction (Hikami *et al.*, 1980) can be ignored and there are no magnetic impurities in the metal, the times τ , τ_φ , and τ_B are the only relevant time scales, and they control the behavior of the low temperature conductivity.

We now extend the previous analysis to graphene. Again, as expected, the chiral nature of the electrons (or, equivalently, their non-trivial Berry's phase) will play a major role. As before, we keep the discussion as elementary as possible.

B. Weak localization in graphene

In graphene, the quasi-exact conservation of the chirality and the existence of two valleys have profound effects in the low-temperature conductivity of the material. Below, we present the general picture of the quantum corrections in graphene, referring the interested reader to the literature for the subtleties appearing under a detailed analysis of this problem (Aleiner and Efetov, 2006; McCann *et al.*, 2006; Morpurgo and Guinea, 2006; Mucicciolo and Lewenkopf, 2010; Suzuura and Ando, 2002).

As shown in Sec. V.A, in a normal metal the only elastic time is the relaxation time τ . In graphene the situation is more complex. In order to understand the complexity of the situation, consider two different matrix elements of a potential created by a given impurity. We assume the potential to have the form

$$V(\mathbf{r}) = \frac{u}{r_0^2 \pi} e^{-r^2/r_0^2}. \quad (39)$$

The range of the potential depends on the value of r_0 : the larger r_0 , the larger the range. The effect of this potential on electrons within the same valley (denoted intra-valley scattering) is given by the matrix element

$$\langle \psi_+(\mathbf{k}') | V(\mathbf{r}) | \psi_+(\mathbf{k}) \rangle = \frac{u}{8A_c} f(\mathbf{k}, \mathbf{k}') e^{-q^2 r_0^2 / 4}, \quad (40)$$

with $f(\mathbf{k}, \mathbf{k}') = \cos[\theta(\mathbf{k})/2 - \theta(\mathbf{k}')/2]$ and $q = |\mathbf{k} - \mathbf{k}'|$. If we take $\epsilon_F = 0.5$ eV one obtains $q \sim 0.2/a$, with $a = \sqrt{3}a_0$. The function $f(\mathbf{k}, \mathbf{k}')$ shows that the scattering is not isotropic in momentum space, a consequence of the chiral nature of electrons in graphene. From $f(\mathbf{k}, \mathbf{k}')$, we also see that the scattering amplitude for backscattering, $f(\mathbf{k}, -\mathbf{k})$, is zero, the fingerprint of Klein tunneling (recall Fig. 3) for massless Dirac electrons (Beenakker, 2008).

If the potential also couples electronic momentum states from \mathbf{K} and \mathbf{K}' valleys (denoted inter-valley scattering) the matrix element, using wave functions from different valleys, reads

$$\langle \psi_+(\mathbf{k}') | V(\mathbf{r}) | \psi_+(\mathbf{k}) \rangle = \frac{u}{8A_c} g(\mathbf{k}, \mathbf{k}') e^{-Q^2 r_0^2/4}, \quad (41)$$

with $g(\mathbf{k}, \mathbf{k}') = i \sin[\theta(\mathbf{k})/2 - \theta(\mathbf{k}')/2]$ and $Q \simeq |\mathbf{K} - \mathbf{K}'| = 4\pi/(3a)$. In this case, backscattering is permitted, $g(\mathbf{k}, -\mathbf{k}) \neq 0$, since scattering couples states in the \mathbf{K} and \mathbf{K}' valleys, which have opposite chirality (recall Fig. 3).

Equation (41) shows that only for very short-range potentials, $r_0 \lesssim a$, does intervalley scattering have a significant amplitude. For long range potentials, only intra-valley scattering plays a role.

From the above discussion it follows that, in the case of graphene, we need to define several elastic scattering times (Aleiner and Efetov, 2006; McCann *et al.*, 2006; Morpurgo and Guinea, 2006):

1. τ_{iv} , representing inter-valley scattering, whose scatterers are very short-range potentials with range $r_0 \lesssim a$, such as some types of adatoms, adsorbed hydrocarbons, or vacancies.
2. τ_s , representing intra-valley scattering, whose scatterers are long range potentials, such as ripples, dislocations, and charged scatterers.
3. τ_w , representing also another contribution to intra-valley scattering. This scattering time has its origin in the fact that chirality is not an exact symmetry of Dirac fermions in graphene (due to trigonal warping effects), therefore allowing for some amount of backscattering within the same valley. The importance of this scattering time grows as the Fermi energy increases.

As long as the scattering potentials are long range, inter-valley scattering is negligible and back-scattering in graphene is absent, except from a small contribution from τ_w . The effect just described is, at the more fundamental level, a consequence of the Berry's phase (of π) acquired by massless Dirac electrons when they perform a closed chiral orbit (Berry and Mondragon, 1987; Mikitik and Sharlai, 1999). The Berry's phase transforms the constructive interference, we described above for normal metals, into a destructive one, leading to weak anti-localization. Under these circumstances, the interference effect seen in Sec. V.A for a normal metal cannot exist in graphene, forward scattering is enhanced and one should expect weak anti-localization effects to manifest themselves, that is, if $\tau_{iv} \gg \tau_\varphi$ we have (ignoring τ_w) (McCann *et al.*, 2006; Suzuura and Ando, 2002)

$$\sigma_{awl} - \sigma_0 > 0, \quad (42)$$

where σ_{awl} represents the enhancement (anti-localizing effect) of the conductivity over Drude's result σ_0 due to Klein tunneling. If short range scatterers are present, then inter-valley scattering plays a role, and since electrons in the \mathbf{K} and \mathbf{K}' valleys have opposite chirality, back-scattering is present [see the function $g(\mathbf{k}, \mathbf{k}')$], and we expect weak localization effects, according to Eq. 37; detailed calculations confirmed this picture (McCann *et al.*, 2006; Suzuura and Ando, 2002). When the effect of a magnetic field is included, the general rigorous expression for the weak localization corrections was derived by two groups independently (Aleiner and Efetov, 2006; McCann *et al.*, 2006), and $\delta\sigma(B)$ can be either positive or negative depending on the relative values of the different scattering times, including τ_B . For a comprehensive discussion of the interplay between the different scattering times and the quantum corrections to the conductivity, the interested reader is referred to the technical literature (Aleiner and Efetov, 2006; Kechedzhi *et al.*, 2007; McCann *et al.*, 2006).

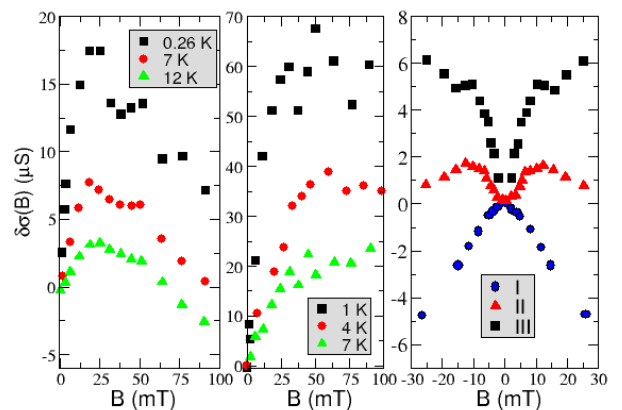


Figure 13 (Color online) The quantity $\delta\sigma(B)$ is defined as in Eq. (38). **Left:** Weak anti-localization behavior (the gate voltage used was $V_g \lesssim 1$ V, corresponding to an electron density $n \lesssim 7 \times 10^{10} \text{ cm}^{-2}$). **Center:** Weak localization behavior (the gate voltage used was $V_g = 11$ V, corresponding to an electron density $n \simeq 8 \times 10^{11} \text{ cm}^{-2}$). **Right:** Dependence of $\delta\sigma(B)$ on the electronic density (it grows from I to III), at $T = 27$ K. A fit of the data must use the rigorous formula derived in the literature (Aleiner and Efetov, 2006; McCann *et al.*, 2006). [Data from F. V. Tikhonenko *et al.* (Tikhonenko *et al.*, 2008, 2009).]

In the left panel of Fig. 13 we show, for small values of the magnetic field, a weak localization dip ($\delta\sigma(B)$ grows) followed by, above a certain field value B^* , weak anti-localization behavior of the conductivity, since $\delta\sigma(B)$ starts to decrease upon increasing the magnetic field over B^* (no saturation of $\delta\sigma(B)$ is measured upon increasing B , as in the weak localization case). In the central panel of Fig. 13, we show weak localization behavior in graphene, since the corrections $\delta\sigma(B)$ never decrease

upon increasing the magnetic field, and tend to saturation. Since the electronic density in the central panel of Fig. 13 is few times larger than that in the left one, it seems that the effect of short-range scatterers is more effective at higher densities (Tikhonenko *et al.*, 2009); at lower densities long-range scatterers dominate. Indeed, in the right panel of Fig. 13, we clearly see a crossover from weak anti-localization to weak localization as the electronic density increases from I to III, at a temperature of 27 K; considering important screening effects of charged impurities at large electronic densities, such a result sounds reasonable. It is a remarkable experimental fact that quantum interference effects just discussed can be observed in graphene at temperatures as high as ~ 200 K (Tikhonenko *et al.*, 2009).

As stated, we expect that in graphene the presence of different kinds of defects (in different concentrations) will control whether weak localization or weak anti-localization is observed. This depends on the relative value of the different elastic times introduced above and on the electron density. A detailed analysis of this point is essential for a correct interpretation of the data, and has been done in great detail (McCann *et al.*, 2006; Morpurgo and Guinea, 2006). The numerical values for the different scattering times can be obtained from the experimental data (Tikhonenko *et al.*, 2008).

Finally, we note that the observation of quantum corrections to the conductivity in graphene seems to depend on the details of the fabrication process, which determines the amount of rippling introduced in the system (Morozov *et al.*, 2006). Routes for suppression of weak (anti-)localization effects have been considered (Khvashchenko, 2006) and this effect was experimentally observed as well (Morozov *et al.*, 2006; Tikhonenko *et al.*, 2008). As in the case of strain discussed in Sec. IV.D, ripples are equivalent to effective gauge fields which break time reversal, leading to the suppression of weak localization effects, within each valley. In the system as a whole (both valleys considered) the full time reversal symmetry is preserved.

VI. THE OPTICAL CONDUCTIVITY OF GRAPHENE IN THE INFRARED TO VISIBLE RANGE OF THE SPECTRUM

In the ensuing sections we discuss the calculation of the percentage of light transmitted by a graphene membrane, when light shines from behind. This property is controlled by the optical conductivity $\sigma(\omega)$ of the material. We analyze how and why the experimental behavior of $\sigma(\omega)$ deviates from the predictions of the independent electron model.

A. Graphene as a transparent membrane

The calculation of light absorption by a given material is equivalent to the calculation of the optical conductivity. In general, such a calculation proceeds using Kubo's formula. In the case of graphene, it is possible to use Fermi's golden rule to obtain directly the fraction of absorbed light, which turns out to be a much simpler calculation than computing the optical conductivity first (Kravets *et al.*, 2010). The central quantity to be computed is the transition rate of electrons excited from the valence band to the conduction one, as shown in Fig. 14.

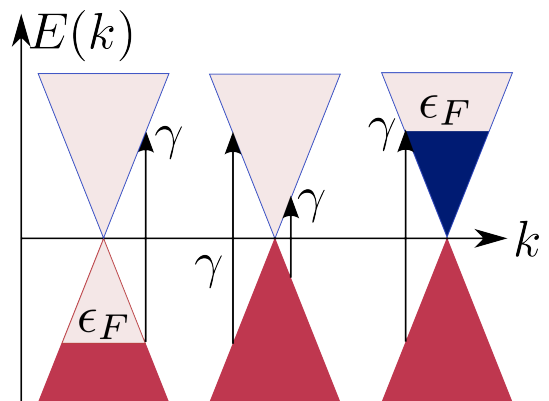


Figure 14 (Color online) Pictorial description of the optical excitation of electrons in graphene. The absorption of a photon can only induce vertical inter-band transitions. From left to right we have graphene doped with holes, neutral, and doped with electrons.

In the presence of a vector potential \mathbf{A} the Dirac Hamiltonian has the form

$$H_{\mathbf{K}} = v_F \boldsymbol{\sigma} \cdot (\mathbf{p} + e\mathbf{A}). \quad (43)$$

We represent the electric field as $\mathbf{E} = -\partial\mathbf{A}/\partial t$ and choose the polarization of the field along the x -axis: $\mathbf{A} = \hat{x}A_0(e^{i\omega t} + e^{-i\omega t})/2$. The term $v_F \boldsymbol{\sigma} \cdot e\mathbf{A}$ will be taken as perturbation, and in the spirit of time dependent perturbation theory, only the exponential with negative exponent is taken. The transitions induced by light absorption are now controlled by the σ_x matrix. Clearly the matrix element $\langle \psi_\lambda | \sigma_x | \psi_\lambda \rangle$ cannot contribute to the conductivity, since light cannot induce transitions within the same band, among states of equal momentum. The only non-vanishing contributing matrix element is therefore $\langle \psi_1 | \sigma_x | \psi_{-1} \rangle = -\frac{i}{2}v_F e A_0 \sin \theta(\mathbf{k})$. The transition rate is then given by Fermi's golden rule:

$$W_{1,-1}(\mathbf{k}) = \frac{2\pi}{4\hbar} v_F^2 e^2 A_0^2 \sin^2 \theta(\mathbf{k}) \delta(2v_F k \hbar - \omega \hbar). \quad (44)$$

The Dirac delta function in Eq. (44) enforces the condition that only electrons with energy $\omega/2$ can be excited to the conduction band. The transitions we are referring to are shown in Fig. 14. To obtain the contribution from

all states we have to integrate over the momentum and multiply the result by four (two for spin times two for valley). The calculations are elementary and the result for the total transition rate per unit area is

$$\frac{1}{\tau} = \frac{e^2 A_0^2 \omega}{8\hbar^2}. \quad (45)$$

If light of frequency ω is shining upon a unit area of graphene, the amount of absorbed power per unit area is $W_a = \hbar\omega/\tau$. The energy flux impinging on graphene is given by $W_i = c\epsilon_0 E_0^2/2$, with $E_0 = A_0\omega$. Therefore the fraction of transmitted light is (Nair *et al.*, 2008)

$$T = 1 - \frac{W_a}{W_i} = 1 - \pi\alpha \simeq 0.977, \quad (46)$$

with $\alpha = e^2/(4\pi\epsilon_0\hbar c)$ the fine structure constant. The absorption of light is therefore independent of frequency and given only by universal constants. The high transmittance of graphene is shown Fig. 15; it is remarkable that a one atom thick membrane can be seen by the naked eye.



Figure 15 (Color online) An optical image of an aperture partially covered with graphene and its bilayer (from left to right: air/graphene/bilayer), taken in a light transmission experiment (courtesy of A. K. Geim).

It follows from the previous analysis that the transmission at finite doping is given by

$$T(\epsilon_F) \approx (1 - \pi\alpha)\theta(\omega - 2\epsilon_F), \quad (47)$$

where the Heaviside step function takes into account that absorption can only occur for frequencies larger than twice the Fermi energy, due to Pauli's principle. The result given by Eq. (46) is identical to the one given by a rigorous calculation based on Kubo's formula (Abergel *et al.*, 2007; Gusynin *et al.*, 2007; Kuzmenko *et al.*, 2008; Peres *et al.*, 2006; Peres and Stauber, 2008). The reason why the perturbative calculation works so well is because the final answer is controlled by the small dimensionless parameter α . The reason why the transmission is controlled by the fine structure constant originates in the

chiral nature of the electrons in graphene, a result extensible to few-layers graphene (Min and MacDonald, 2009).

It is now a simple matter to include corrections to the linear spectrum of graphene in the formalism (the conical nature of the spectrum is valid for energies of the order of $\lesssim 1$ eV). The addition of a next-nearest neighbor hopping term can also be included and treated within this formalism. The case of a next-nearest neighbor hopping is actually trivial, being proportional to the identity matrix its contribution is zero. In fact, it is proven in general (Stauber *et al.*, 2008b) that the contribution of the next-nearest neighbor hopping only enters in the final result as a renormalization of the energy spectrum.

As stated, the transmittance of light through graphene can be computed from a previous knowledge of the optical conductivity of the material. The transmittance is calculated from the solution of Fresnel's equations, reading (Abergel *et al.*, 2007; Blake *et al.*, 2007; Pedersen, 2003; Stauber *et al.*, 2008b)

$$T = |1 + \sigma(\omega)/(2c\epsilon_0)|^{-2}, \quad (48)$$

where $\sigma(\omega)$ is the optical conductivity (Falkovsky and Pershoguba, 2007; Falkovsky and Varlamov, 2007; Gusynin and Sharapov, 2005; Gusynin *et al.*, 2007, 2009; Peres *et al.*, 2006; Stauber *et al.*, 2008b) of graphene, given, at zero temperature and within the independent electron approximation, by ($\epsilon_F > 0$)

$$\sigma(\omega) = \sigma_0\theta(\omega\hbar - 2\epsilon_F) + i\sigma_0\frac{4\epsilon_F}{\pi\omega\hbar} - i\frac{\sigma_0}{\pi}\ln\frac{|\hbar\omega + 2\epsilon_F|}{|\hbar\omega - 2\epsilon_F|}. \quad (49)$$

The quantity $\sigma_0 = \pi e^2/(2h)$ is termed the ac universal conductivity of graphene. Inserting Eq. (49) into Eq. (48) and taking $\epsilon_F = 0$ we obtain the result of Eq. (46). Working the other way around, using Eq. (47) in Eq. (48), we obtain for neutral graphene $\sigma(\omega) = \sigma_0$, in accordance with Eq. (49). The fact that for neutral graphene $\sigma(\omega)$ is given in terms of universal constants only, with no reference to any of the material parameters, is a rare result in condensed matter physics. If the intensity of light impinging on graphene is *large*, then non-linear corrections to T start to play a role, which is expected to lead to an increase of the transmittance (Mishchenko, 2009; Rosenstein *et al.*, 2010). The non-linear optical susceptibility coefficients of graphene have recently been measured using four-wave mixing (Hendry *et al.*, 2010).

Due to its high transmittance, graphene can be used as transparent conductive electrodes in solar cells and liquid crystal devices (LCD) (Bae *et al.*, 2010; Blake *et al.*, 2008; Wang *et al.*, 2008).

B. The optical conductivity of neutral graphene

We now discuss the experimental results for the optical conductivity of neutral graphene and how those mea-

measurements deviate from the independent electron model presented above.

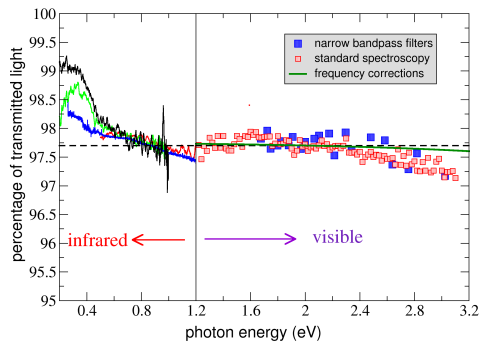


Figure 16 (Color online) Transmittance of graphene. For photon energies below 1.2 eV, we plot data from reflectance measurements taken by K. Fai Mak *et al.* (Mak *et al.*, 2008); different curves correspond to different graphene devices (courtesy of F. Kin Mak). For photon energies larger than 1.2 eV, we plot data from two different types of measurements (Nair *et al.*, 2008): narrow bandpass filters, with a full band width at half maximum of 10 nm, and standard spectroscopy measurements. The dashed line is the result of Eq. (46). The solid (green) line, to the right of 1.2 eV, is a plot of T obtained from a calculation of the conductivity, including trigonal warping corrections (Stauber *et al.*, 2008b).

In Fig. 16 we show measurements from two different groups (Mak *et al.*, 2008; Nair *et al.*, 2008) in two different regions of the spectrum. For photon energies E_γ below 1.2 eV (in the near infrared region), the data were taken from reflectance measurements, at room temperature. The absorbance of the different samples is spectrally flat within a band of 10%. Roughly speaking, the transmittance follows the value given by Eq. (46). A more detailed analysis shows that the transmittance below $E_\gamma < 0.5$ eV increases over the universal value, whereas closer to $E_\gamma \lesssim 1.2$ eV it decreases slightly from that value. According to Mak *et al.* (Mak *et al.*, 2008), and for energies $E_\gamma < 0.5$ eV, both temperature effects and some amount of variable extrinsic doping decrease the conductivity and therefore produce an increase in the transmittance. In other words, if light absorption decreases, then the transmittance increases. This effect is equivalent to a finite chemical potential (having effectively a Pauli's principle based blocking effect), which contributes to an increase in the transmittance. The temperature effect that they (Mak *et al.*, 2008) used in their argument, was predicted to be of importance at room temperature and energies below 0.5 eV for undoped graphene (Peres and Stauber, 2008), in agreement with the experimental measurements. Additionally, this set of measurements showed that the optical conductivity of graphene can also be affected by unavoidable doping and intra-band scattering. Indeed, a SCBA (Peres *et al.*,

2006) calculation of the conductivity of graphene at zero temperature and zero doping showed that $\sigma(\omega)$ departs from its universal value, $\sigma_0 = \pi e^2/(2h)$, being strongly reduced at low frequencies, due to disorder.

In conclusion, the deviation of the transmittance of graphene from the universal value predicted for Dirac fermions is a way of gaining insight on other electronic effects present in the material (Li *et al.*, 2008b).

Figure 16 also shows the transmittance of graphene in the photon energy range 1.2–3 eV. The measured value follows the prediction of Eq. (46), except at energies around 3 eV, where absorption increases. Since at energies as large as 3 eV the electronic energy dispersion deviates considerably from the Dirac cone approximation – an effect known as trigonal warping – a calculation taking into account trigonal warping corrections to the band structure of graphene was performed (Nair *et al.*, 2008; Stauber *et al.*, 2008b), and the result is given by the solid line in Fig. 16. The calculation does predict an increase in light absorption at energies around 3 eV (an effect opposite to that discussed above for energies $E_\gamma < 0.5$ eV), but falls short on accounting for the magnitude of the effect. Within the independent electron model, the computed enhancement of the conductivity is essentially due to the increase in the density of states as the Van Hove singularity is approached, which is located at the energy of ~ 2.7 eV. Thus, transitions between states located at the Van Hove singularities of the valence and the conduction bands require photons of energy ~ 5.4 eV. Optical experiments using photons of about this energy have confirmed the strong enhancement of light absorption due to the Van Hove singularities (Kravets *et al.*, 2010).

Two possible additional causes for such an increase in the absorption come to mind: contamination of the sample due to some organic residues (originated from the exfoliation process) or/and many-body effects (Herbut *et al.*, 2008; Mishchenko, 2008). A recent calculation, however, showed that electron-electron interactions correct the transmission (reducing it) by only 0.03 – 0.04% (Katsnelson, 2008; Sheehy and Schmalian, 2007, 2009). On the other hand, in the regime of energies relevant for the visible range of the spectrum, the fine structure constant of graphene α_g is a number of order 1, a fact casting reasonable doubts on the validity of any perturbative calculation.

A recent *ab initio* calculation (Yang *et al.*, 2009) used the Kohn-Sham eigenvalues and eigenvectors to compute the optical conductivity of graphene from infrared to visible frequencies. This type of mean-field calculations includes electron-electron interactions by means of the exchange and correlation approximations. The optical conductivity obtained does not fit exactly the data of Fig. 16, since it predicts an absorption higher than what is measured experimentally, in the full frequency range. Nevertheless, the proposed excitonic effects (included via

the solution of the Bethe-Salpeter equation) were shown to account well for the experimental deviations (to lower energies) in the enhancement in light absorption for photon energies associated with transitions between states located at the Van Hove singularities of the valence and the conduction bands (Kravets *et al.*, 2010) relatively to the predictions made by the non-interacting electrons theory. Indeed, the elementary theory predicts an intense absorption peak at about 5.2 eV, whereas the measured data shows a red shift of the peak to 4.6 eV. The discrepancy can be solved by considering the mutual attraction of the electron-hole pair, created at the two Van Hove singularities, when a photon of the right frequency is absorbed.

The energy red-shift mentioned is easy to understand from the point of view of the mutual attraction of the electron-hole pair (forming an exciton): since the electron and hole have opposite charges, the effective energy seen by the photon being absorbed is the non-interacting value minus a positive correction coming from the electrostatic attraction between the electron and the hole created by the absorption of the photon.

C. The optical conductivity of gated graphene

Measurements of the optical conductivity of gated graphene, in the far infrared region of the spectrum (Li *et al.*, 2008b), also show strong deviations from the simple theory given above, and expressed in concise form by Eq. (49).

The deviations seen in the data (Li *et al.*, 2008b), for all values of the gate-voltage considered in the experiment (ranging from $V_g = 10$ to 71 V), are of five different types: (i) finite absorption below 2μ , which is due to both inter-band and intra-band elastic and inelastic scattering processes; (ii) broadening of the absorption edge around the energy threshold 2μ ; (iii) an enhancement of the conductivity above the universal value σ_0 in the energy range between 2μ and $2\mu + E^*$, where E^* is a characteristic energy scale, (iv) a reduction of the conductivity below σ_0 , at energies above E^* , with the conductivity as a function of frequency having a positive curvature, and (v) the imaginary part of the conductivity is larger than the value predicted by the non-interacting model for energies $\hbar\omega \gg 2\mu$.

Additionally, we point out that the optical conductivity curves measured experimentally (Li *et al.*, 2008b) collapse on top of each other when re-plotted as function of ω/μ , implying that the mechanism causing deviations from the non-interacting approximation must be intrinsic.

To explain all measured deviations, it is necessary to take into account disorder, temperature, electronic density inhomogeneities (Zhang *et al.*, 2009), and electron-electron interaction effects, of excitonic nature (Peres

et al., 2010). In Fig. 17 we show one set of the measured data (solid blue curve), together with calculations using two models: (i) a model where the independent electron theory is supplemented with the effect of disorder (computed with the two models discussed in Sec. IV.A) and (ii) a calculation including excitonic effects on top of model (i). It is clear that the first one, considering only disorder, does not account for the five deviations observed in the data, relatively to the independent electron model; it partially accounts for the enhancement of the conductivity below 2μ . The additional optical response observed in the data, in this frequency range, must come from intra-band scattering processes (Grushin *et al.*, 2009), not included in model (i). Points (ii)–(v) are all accounted for by including excitonic effects, that is, model (ii). There is, however, the need to use in the model a higher temperature, $T = 120$ K, than that measured experimentally by the finger of the cryostat, $T = 54$ K. This can be justified by recalling that graphene is a system presenting small inhomogeneities of the electronic density. This fact effectively smears the chemical potential and such an effect can be accounted for by considering an effective higher temperature, as was shown to be the case in the interpretation of the optical response of graphene's bilayer (Kuzmenko *et al.*, 2009).

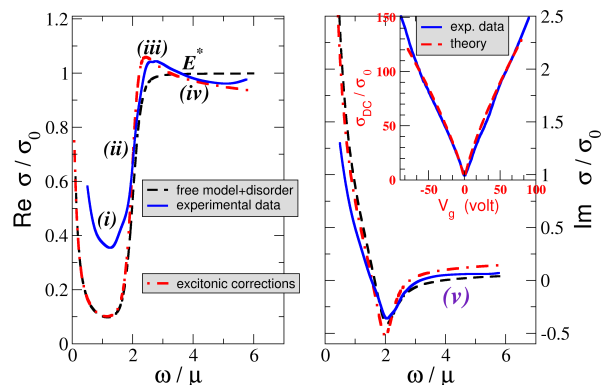


Figure 17 (Color online) Optical conductivity of gated graphene on top of silicon oxide, in units of σ_0 . The data is given by the solid curve. The dashed curve is a calculation taking disorder into account, and the dot-dashed curve is a calculation including disorder and electron-electron interactions. The experimental curves refer to a gate voltage of 28 V, which corresponds a Fermi energy of $\mu \simeq 0.18$ eV. The calculation took an effective temperature of 120 K. In the **left(right)** panel we have the real(imaginary) part of the conductivity. In the **inset**, the measured dc conductivity of the device (solid curve) depicted together with a fit of $\sigma(\epsilon_F)$ using Eqs. (20) and (25). The fit of the dc conductivity fixes the concentration of impurities to the values of $n_i = 2 \times 10^{11}$ cm $^{-2}$, for resonant scatterers, and $n_i = 1 \times 10^{11}$ cm $^{-2}$, for charged ones (dashed curve). (Data from Z. Li *et al.* (Li *et al.*, 2008b), courtesy of Zhiqiang Li.)

In the same set of measurements (Li *et al.*, 2008b), an increase in the Fermi velocity over the value 1.1×10^6 m/s was measured, upon diminishing the gate voltage. The renormalized Fermi velocity, due to exchange, was predicted to be (including the Thomas-Fermi screening of the Coulomb potential)

$$v_F = v_{\text{bare}} + \frac{e^2}{4\pi\epsilon_0\epsilon_d\hbar} \left(\ln \frac{2q_c}{9k_F} - \frac{1}{3} \right), \quad (50)$$

where v_{bare} is the bare Fermi velocity, and therefore not an observable parameter, $q_c \sim 1 \text{ \AA}^{-1}$ a cutoff momentum, and we have used the fact that the Thomas-Fermi screening momentum is for graphene on silicon oxide given by $q_{\text{TF}} \simeq 2k_F$ [we note that Eq. (50) is an extension, taking screening into account, of previous results (González *et al.*, 1996; Hwang *et al.*, 2007; Polini *et al.*, 2007)]. The result (50) does show that v_F increases upon decreasing k_F , but the formula fails to fit the data (Li *et al.*, 2008b) over the measured gate voltage range, especially for larger V_g . Alternatively, phonons also seem to partially account for the Fermi velocity renormalization seen in the experiments (Gusynin *et al.*, 2009; Peres *et al.*, 2008; Stauber *et al.*, 2008a).

The renormalization of the Fermi velocity suggests that contributions from many-body effects can be important, but an experiment with a higher degree of accuracy should be repeated, since cyclotron mass measurements (Novoselov *et al.*, 2005a) do not see deviations of the Fermi velocity from $v_F \simeq 1.1 \times 10^6$ m/s upon varying the electronic density.

Finally, we note that, as in the case of neutral graphene discussed in Sec. VI.B, the electron-hole pair mutual-attraction also induces a shift in the Fermi edge at $\omega = 2\mu$ toward lower energies (red shift effect), since, as before, it renormalizes the non-interacting energies by adding a negative number.

In conclusion, the optical response of graphene is a property of the material where different kinds of quantum effects seem to play an important role, all on equal footing. Exploring graphene for nanophotonic devices surely requires a detailed understanding of its optical properties.

VII. CONCLUSIONS

We have given an introductory review on the transport properties of graphene, touching the relevant aspects of this topic. A survey of the literature was given along with a discussion of elementary models, which, despite their simplicity, are in good quantitative agreement with many features of the data. Many of these models were discussed in greater detail in the literature (to which due credit is given), but using more formal methods. We hope that the topics discussed in this Colloquium may contribute to

a wider dissemination of the physics of graphene among the non-specialized audience.

ACKNOWLEDGMENTS

I have benefited immensely from discussions with many colleagues and friends in the last few years, but I would like to thank especially, Aires Ferreira, Andre Geim, Antonio Castro Neto, Bruno Uchoa, Eduardo Castro, Eduardo Mucciolo, Fernando Sols, Francisco Guinea, Jaime Santos, João Lopes dos Santos, Johan Nilsson, José Carlos Gomes, Konstantin Novoselov, Maria Vozmediano, Mikhail Vasilevskiy, Ricardo Ribeiro, Shan-Wen Tsai, Tobias Stauber, Vitor Pereira, and Yuliy Bludov. I also would like to thank the anonymous referees since their comments were most useful to improve the final version of the paper. The hospitality of the National University of Singapore (NUS) is acknowledge, where this work was started. A special thanks goes to ALCRP, FCRP, and MAIC, for their continuous support.

REFERENCES

- Abergel, D. S. L., A. Russell, and V. I. Fal'ko, 2007, *Appl. Phys. Lett.* **91**, 063125.
- Abrikosov, A. A., 1988, *Fundamentals of the Theory of Metals* (North-Holland).
- Adam, S., E. H. Hwang, and S. Das Sarma, 2008, *Physica E* **40**, 1022.
- Adam, S., E. H. Hwang, V. Galitski, and S. Das Sarma, 2007, *Proc. Natl. Acad. Sci.* **104**, 18392.
- Akhmerov, A. R., and C. W. J. Beenakker, 2008, *Phys. Rev. B* **77**, 085423.
- Aleiner, I. L., and K. B. Efetov, 2006, *Phys. Rev. Lett.* **97**, 236801.
- Ando, T., and T. Nakanishi, 1998, *J. Phys. Soc. Jpn.* **67**, 1704.
- Araújo, M. A. N., and N. M. R. Peres, 2006, *J. Phys.: Cond. Matt.* **18**, 1769.
- Bae, S., H. Kim, Y. Lee, X. Xu, J.-S. Park, Y. Zheng, J. Balakrishnan, T. Lei, H. R. Kim, Y. I. Song, Y.-J. Kim, K. S. Kim, B. Özyilmaz, J.-H. Ahn, B. H. Hong, , and S. Iijima, 2010, *Nature Nanotechnology* **5**, 574.
- Bao, W., F. Miao, Z. Chen, H. Zhang, W. Jang, C. Dames, and C. N. Lau, 2009, *Nature Nanotechnology* **4**, 562.
- Bardarson, J. H., J. Tworzydło, P. W. Brouwer, and C. W. J. Beenakker, 2007, *Phys. Rev. Lett.* **99**, 106801.
- Basko, D. M., 2008, *Phys. Rev. B* **78**, 125418.
- Beenakker, C. W., 2008, *Rev. Mod. Phys.* **80**, 1337.
- Beenakker, C. W., and H. Houten, 1991, "Solid state physics," Chap. Quantum Transport in Semiconductor Nanostructure (Academic Press) pp. 1–170.
- Bena, C., and S. A. Kivelson, 2005, *Phys. Rev. B* **72**, 125432.
- Berry, M. V., and R. J. Mondragon, 1987, *Proc. R. Soc. Lond. A* **412**, 53.
- Blake, P., P. D. Brimicombe, R. R. Nair, T. J. Booth, D. Jiang, F. Schedin, L. A. Ponomarenko, S. V. Morozov, H. F. Gleeson, E. W. Hill, A. K. Geim, and K. S. Novoselov, 2008, *Nano Lett.* **8**, 1704.

- Blake, P., K. S. Novoselov, A. H. Castro Neto, D. Jiang, R. Yang, T. J. Booth, A. K. Geim, and E. W. Hill, 2007, *Appl. Phys. Lett.* **91**, 063124.
- Blake, P., R. Yang, S. V. Morozov, F. Schedin, L. A. Ponomarenko, A. A. Zhukov, I. V. Grigorieva, K. S. Novoselov, and A. K. Geim, 2009, *Solid State Commun.* **149**, 1068.
- Bolotin, K. I., F. Ghahari, M. D. Shulman, H. L. Stormer, and P. Kim, 2009, *Nature* **462**, 196.
- Bolotin, K. I., K. J. Sikes, J. Hone, H. L. Stormer, and P. Kim, 2008a, *Phys. Rev. Lett.* **101**, 096802.
- Bolotin, K. I., K. J. Sikes, Z. Jiang, M. Klima, G. Fudenberg, J. Hone, P. Kim, and H. L. Stormer, 2008b, *Solid State Communications* **146**, 351.
- Booth, T. J., P. Blake, R. R. Nair, D. Jiang, E. W. Hill, U. Bangert, A. Bleloch, M. Gass, K. S. Novoselov, M. I. Katsnelson, and A. K. Geim, 2008, *Nano Lett.* **8**, 2442.
- Castro, E. V., K. S. Novoselov, S. V. Morozov, N. M. R. Peres, J. Lopes dos Santos, J. Nilsson, F. Guinea, A. K. Geim, and A. H. Castro Neto, 2007, *Phys. Rev. Lett.* **99**, 216802.
- Castro Neto, A. H., 2010, *Materials Today* **13**, 12.
- Castro Neto, A. H., and F. Guinea, 2009, *Phys. Rev. Lett.* **103**, 026804.
- Castro Neto, A. H., F. Guinea, and N. M. R. Peres, 2006, *Physics World* **11**, 33.
- Castro Neto, A. H., F. Guinea, N. M. R. Peres, K. S. Novoselov, and A. K. Geim, 2009, *Rev. Mod. Phys.* **81**, 109.
- Chakravarty, S., and A. Schmid, 1986, *Phys. Rep.* **140**, 193.
- Cheianov, V. V., and V. I. Fal'ko, 2006, *Phys. Rev. B* **74**, 041403.
- Cheianov, V. V., V. I. Fal'ko, B. L. Altshuler, and I. L. Aleiner, 2007, *Phys. Rev. Lett.* **99**, 176801.
- Cheianov, V. V., O. Syljuasen, B. L. Altshuler, and V. I. Fal'ko, 2010, *Europhys. Lett.* **89**, 56003.
- Chen, J.-H., W. G. Cullen, C. Jang, M. S. Fuhrer, and E. D. Williams, 2009, *Phys. Rev. Lett.* **102**, 236805.
- Chen, J. H., C. Jang, M. S. Fuhrer, E. D. Williams, and M. Ishigami, 2008, *Nature Phys.* **4**, 377.
- Christillin, P., and E. d'Emilio, 2007, *Phys. Rev. A* **76**, 042104.
- Connolly, M. R., K. L. Chiou, C. G. Smith, D. Anderson, G. A. C. Jones, A. Lombardo, A. Fasoli, and A. C. Ferrari, 2010, *Appl. Phys. Lett.* **96**, 113501.
- Danneau, R., F. Wu, M. F. Craciun, S. Russo, M. Y. Tomi, J. Salmilehto, A. F. Morpurgo, and P. J. Hakonen, 2008, *Phys. Rev. Lett.* **100**, 196802.
- Delahaye, F., and B. Jeckelmann, 2003, *Metrologia* **40**, 217.
- Dominguez-Adamé, F., 1990, *J. Phys. A: Math. Gen.* **23**, 1993.
- Dóra, B., K. Ziegler, and P. Thalmeier, 2008, *Phys. Rev. B* **77**, 115422.
- Du, X., I. Skachko, A. Barker, and E. Y. Andrei, 2008, *Nature Nanotechnology* **3**, 491.
- Du, X., I. Skachko, F. Duerr, A. Luican, and E. Y. Andrei, 2009, *Nature* **462**, 192.
- Dubois, S.-M., Z. Zanolli, X. Declerck, and J.-C. Charlier, 2009, *Eur. Phys. J. B* **72**, 1.
- Elias, D. C., R. R. Nair, T. M. G. Mohiuddin, S. V. Morozov, P. Blake, M. P. Halsall, A. C. Ferrari, D. W. Boukhvalov, M. I. Katsnelson, A. K. Geim, and K. S. Novoselov, 2009, *Science* **323**, 610.
- Falkovsky, L. A., and S. S. Pershoguba, 2007, *Phys. Rev. B* **76**, 153410.
- Falkovsky, L. A., and A. A. Varlamov, 2007, *Eur. Phys. J. B* **56**, 281.
- Faugeras, C., B. Faugeras, M. Orlita, M. Potemski, R. R. Nair, and A. K. Geim, 2010, *ACS Nano* **4**, 1889.
- Ferralis, N., R. Maboudian, and C. Carraro, 2008, *Phys. Rev. Lett.* **101**, 156801.
- Ferry, D. K., S. M. Goodnick, and J. Bird, 2009, *Transport in Nanostructures*, 2nd ed. (Cambridge).
- Fogler, M. M., 2009, *Phys. Rev. Lett.* **103**, 236801.
- Fogler, M. M., A. H. Castro Neto, and F. Guinea, 2010, *Phys. Rev. B* **81**, 161408(R).
- Fogler, M. M., F. Guinea, and M. I. Katsnelson, 2008, *Phys. Rev. Lett.* **101**, 226804.
- Fuhrer, M. S., G. N. Lau, and A. H. MacDonald, 2010, *MRS Bulletin* **35**, 289.
- Gallagher, P., K. Todd, and D. Goldhaber-Gordon, 2010, *Phys. Rev. B* **81**, 115409.
- Geim, A. K., 2009, *Science* **324**, 1530.
- Geim, A. K., and P. Kim, 2008, *Scientific American* **298**, 68.
- Geim, A. K., and A. H. MacDonald, 2007, *Physics Today* **60**, 35.
- Geim, A. K., and K. S. Novoselov, 2007, *Nature Materials* **6**, 183.
- Giesbers, A. J. M., G. Rietveld, E. Houtzager, U. Zeitler, R. Yang, K. S. Novoselov, A. K. Geim, and J. C. Maan, 2008, *Appl. Phys. Lett.* **93**, 222109.
- González, J., F. Guinea, and M. A. H. Vozmediano, 1996, *Phys. Rev. Lett.* **77**, 3589.
- González, J., F. Guinea, and M. A. H. Vozmediano, 1999, *Phys. Rev. B* **59**, R2474.
- Grushin, A. G., B. Valenzuela, and M. A. H. Vozmediano, 2009, *Phys. Rev. B* **80**, 155417.
- Guinea, F., M. I. Katsnelson, and A. K. Geim, 2010, *Nature Phys.* **6**, 30.
- Gusynin, V. P., and S. G. Sharapov, 2005, *Phys. Rev. Lett.* **95**, 146801.
- Gusynin, V. P., S. G. Sharapov, and J. P. Carbotte, 2007, *Int. Jour. of Mod. Phys. B* **21**, 4611.
- Gusynin, V. P., S. G. Sharapov, and J. P. Carbotte, 2009, *New J. Phys.* **11**, 095013.
- Han, M. Y., J. C. Brant, and P. Kim, 2010, *Phys. Rev. Lett.* **104**, 056801.
- Han, M. Y., B. Oezylmaz, Y. Zhang, and P. Kim, 2007, *Phys. Rev. Lett.* **98**, 206805.
- Hasegawa, Y., R. Konno, H. Nakano, and M. Kohmoto, 2006, *Phys. Rev. B* **74**, 033413.
- Hendry, E., P. J. Hale, J. Moger, A. K. Savchenko, and S. A. Mikhailov, 2010, *Phys. Rev. Lett.* **105**, 097401.
- Hentschel, M., and F. Guinea, 2007, *Phys. Rev. B* **76**, 115407.
- Herbut, I. F., V. Juričić, and O. Vafek, 2008, *Phys. Rev. Lett.* **100**, 046403.
- Hikami, S., A. I. Larkin, and Y. Nagaoka, 1980, *Prog. Theor. Phys.* **63**, 707.
- Hong, X., K. Zou, and J. Zhu, 2009, *Phys. Rev. B* **80**, 241415.
- Huang, B., M. Liu, N. Su, J. Wu, W. Duan, B. Gu, and F. Liu, 2009, *Phys. Rev. Lett.* **102**, 166404.
- Huard, B., N. Stander, J. A. Sulpizio, and D. Goldhaber-Gordon, 2008, *Phys. Rev. B* **78**, 121402R.
- Hwang, E. H., and S. Das Sarma, 2007, *Phys. Rev. B* **76**, 195421.
- Hwang, E. H., and S. Das Sarma, 2008, *Phys. Rev. B* **77**, 195412.
- Hwang, E. H., B. Y. Hu, and S. Das Sarma, 2007, *Phys. Rev. Lett.* **99**, 226801.

- Hýtch, M., F. Houdellier, F. Hüe, and E. Snoeck, 2008, *Nature* **453**, 1086.
- Jackiw, R., 1984, *Phys. Rev. D* **29**, 2375.
- Jang, C., S. Adam, J.-H. Chen, E. D. Williams, S. D. Sarma, and M. S. Fuhrer, 2008, *Phys. Rev. Lett.* **101**, 146805.
- Jiang, Z., E. A. Henriksen, L. C. Tung, Y.-J. Wang, M. E. Schwartz, M. Y. Han, P. Kim, and H. L. Stormer, 2007, *Phys. Rev. Lett.* **98**, 197403.
- Jiao, L., X. Wang, G. Diankov, H. Wang, and H. Dai, 2010, *Nature Nanotechnology* **5**.
- Johnson, M. H., and B. A. Lippmann, 1949, *Phys. Rev.* **76**, 828.
- de Juan, F., A. Cortijo, and M. A. H. Vozmediano, 2007, *Phys. Rev. B* **76**, 165409.
- Katoch, J., J. Chen, R. Tsuchikawa, C. W. Smith, E. R. Mucciolo, and M. Ishigami, 2010, *Phys. Rev. B* **82**, 081417(R).
- Katsnelson, M. I., 2006, *Eur. Phys. J. B* **51**, 157.
- Katsnelson, M. I., 2007, *Materials Today* **10**, 20.
- Katsnelson, M. I., 2008, *Europhys. Lett.* **84**, 37001.
- Katsnelson, M. I., and A. K. Geim, 2008, *Phil. Trans. R. Soc. A* **366**, 195.
- Katsnelson, M. I., F. Guinea, and A. K. Geim, 2009, *Phys. Rev. B* **79**, 195426.
- Katsnelson, M. I., and K. S. Novoselov, 2007, *Solid State Commun.* **143**, 3.
- Katsnelson, M. I., K. S. Novoselov, and A. K. Geim, 2006, *Nature Phys.* **2**, 620.
- Kechedzhi, K., E. McCann, V. I. Fal'ko, H. Suzuura, T. Ando, and B. L. Altshuler, 2007, *Eur. Phys. J. Special Topics* **148**, 39.
- Khveshchenko, D. V., 2006, *Phys. Rev. Lett.* **97**, 036802.
- Kim, E.-A., and A. H. Castro Neto, 2008, *Europhys. Lett.* **84**, 57007.
- Kim, K. S., Y. Zhao, H. Jang, S. Y. Lee, J. M. Kim, K. S. Kim, J.-H. Ahn, P. Kim, J.-Y. Choi, and B. H. Hong, 2009, *Nature* **457**, 706.
- Klos, J. W., and I. V. Zozoulenko, 2010, *Phys. Rev. B* **82**, 081414(R).
- Kosynkin, D. V., A. L. Higginbotha, A. Sinitskiil, J. R. Lomeda, A. Dimiev, B. K. Price, and J. M. Tour, 2009, *Nature* **458**, 872.
- Kravets, V. G., A. N. Grigorenko, R. R. Nair, P. Blake, S. Anissimova, K. S. Novoselov, and A. K. Geim, 2010, *Phys. Rev. B* **81**, 155413.
- Kuzmenko, A. B., I. Crassee, D. van der Marel, P. Blake, and K. S. Novoselov, 2009, *Phys. Rev. B* **80**, 165406.
- Kuzmenko, A. B., E. van Heumen, F. Carbone, and D. van der Marel, 2008, *Phys. Rev. Lett.* **100**, 117401.
- Lahiri, J., Y. Lin, P. Bozkurt, I. I. Oleynik, and M. Batzill, 2010, *Nature Nanotechnology* **5**, 326.
- Landau, L. D., L. P. Pitaevskii, and E. M. Lifshitz, 1984, *Electrodynamics of Continuous Media*, 2nd ed. (Pergamon).
- Levy, N., S. A. Burke, K. L. Meaker, M. Panlasigui, A. Zettl, F. Guinea, A. H. C. Neto, and M. F. Crommie, 2010, *Science* **329**, 5991.
- Lewenkopf, C. H., E. R. Mucciolo, and A. H. Castro Neto, 2008, *Phys. Rev. B* **77**, 081410R.
- Li, G., and E. Y. Andrei, 2007, *Nature Phys.* **3**, 623.
- Li, G., A. Luican, and E. Y. Andrei, 2009, *Phys. Rev. Lett.* **102**, 176804.
- Li, X., X. Wang, L. Zhang, S. Lee, and H. Dai, 2008a, *Science* **319**, 1229.
- Li, Z. Q., E. A. Henriksen, Z. Jiang, Z. Hao, M. C. Martin, P. Kim, H. L. Stormer, and D. N. Basov, 2008b, *Nature Phys.* **4**, 532.
- Liao, L., Y.-C. Lin, M. Bao, R. Cheng, J. Bai, Y. Liu, Y. Qu, K. L. Wang, Y. Huang, and X. Duan, 2010, *Nature*.
- Lin, Q.-G., 1997, *Am. J. Phys.* **65**, 1007.
- Lin, Q.-G., 1999, *Phys. Lett. A* **260**, 17.
- Lin, Y.-M., C. Dimitrakopoulos, K. A. Jenkins, D. B. Farmer, H.-Y. Chiu, A. Grill, and P. Avouris, 2010, *Science* **327**, 5966.
- Lu, Y., B. R. Goldsmith, N. J. Kybert, and A. T. C. Johnson, 2010, *Appl. Phys. Lett.* **97**, 083107.
- Mahan, G. D., 2000, *Many-pARTICLE Physics*, 3rd ed. (Springer).
- Mak, K. F., M. Y. Sfeir, Y. Wu, C. H. Lui, J. A. Misewich, and T. F. Heinz, 2008, *Phys. Rev. Lett.* **101**, 196405.
- Martin, J., N. Akerman, G. Ulbricht, T. Lohmann, J. H. Smet, K. von Klitzing, and A. Yacoby, 2008, *Nature Phys.* **4**, 144.
- Martinazzo, R., S. Casolo, and G. F. Tantardini, 2010, *Phys. Rev. B* **81**, 245420.
- Martino, A. D., L. Dell'Anna, and R. Egger, 2007, *Phys. Rev. Lett.* **98**, 066802.
- McCann, E., 2006, *Phys. Rev. B* **74**, 161403(R).
- McCann, E., and V. I. Fal'ko, 2006, *Phys. Rev. Lett.* **96**, 086805.
- McCann, E., K. Kechedzhi, V. I. Fal'ko, H. Suzuura, T. Ando, and B. Altshuler, 2006, *Phys. Rev. Lett.* **97**, 146805.
- Meyer, J. C., A. K. Geim, M. I. Katsnelson, K. S. Novoselov, T. J. Booth, and S. Roth, 2007, *Nature* **446**, 60.
- Meyer, J. C., C. O. Girit, M. F. Crommie, and A. Zettl, 2008, *Nature* **454**, 319.
- Miao, F., S. Wijeratne, Y. Zhang, U. C. Coskun, W. Bao, and C. N. Lau, 2007, *Science* **317**, 1530.
- Mikitik, G. P., and Y. V. Sharlai, 1999, *Phys. Rev. Lett.* **82**, 2147.
- Min, H., and A. H. MacDonald, 2009, *Phys. Rev. Lett.* **103**, 067402.
- Mishchenko, E. G., 2008, *Europhys. Lett.* **83**, 17005.
- Mishchenko, E. G., 2009, *Phys. Rev. Lett.* **103**, 246802.
- Mohiuddin, T. M. G., A. Lombardo, R. R. Nair, A. Bonetti, G. Savini, R. Jalil, N. Bonini, D. Basko, C. Galiotis, N. Marzari, K. S. Novoselov, A. K. Geim, and A. C. Ferrari, 2009, *Phys. Rev. B* **79**, 205433.
- Montambaux, G., F. Piéchon, J.-N. Fuchs, and M. O. Goerbig, 2009, *Phys. Rev. B* **80**, 153412.
- Monteverde, M., C. Ojeda-Aristizabal, R. Weil, M. Ferrier, S. Gueron, H. Bouchiat, J. N. Fuchs, and D. Maslov, 2010, *Phys. Rev. Lett.* **104**, 126801.
- Morozov, S. V., K. S. Novoselov, M. I. Katsnelson, F. Schedin, D. C. Elias, J. Jaszczak, and A. K. Geim, 2008, *Phys. Rev. Lett.* **100**, 016602.
- Morozov, S. V., K. S. Novoselov, M. I. Katsnelson, F. Schedin, L. A. Ponomarenko, D. Jiang, and A. K. Geim, 2006, *Phys. Rev. Lett.* **97**, 016801.
- Morpurgo, A. F., 2009, *Nature* **462**, 170.
- Morpurgo, A. F., and F. Guinea, 2006, *Phys. Rev. Lett.* **97**, 196804.
- Mucciolo, E. R., A. H. Castro Neto, and C. H. Lewenkopf, 2009, *Phys. Rev. B* **79**, 075407.
- Mucciolo, E. R., and C. H. Lewenkopf, 2010, *J. of Phys.: Cond. Matt.*
- Mueller, T., F. Xia, and P. Avouris, 2010, *Nature Photonics* **4**, 297.
- Müller, M., M. Brüninger, and B. Trauzettel, 2009, *Phys. Rev. Lett.* **103**, 196801.

- Nair, R. R., P. Blake, A. N. Grigorenko, K. S. Novoselov, T. J. Booth, T. Stauber, N. M. R. Peres, and A. K. Geim, 2008, *Science* **320**, 1308.
- Narozhny, B. N., 2007, *Phys. Rev. B* **76**, 153409.
- Nazarov, Y. V., and Y. M. Blanter, 2009, *Quantum Transport: Introduction to Nanoscience* (Cambridge University Press).
- Neugebauer, P., M. Orlita, C. Faugeras, A.-L. Barra, and M. Potemski, 2009, *Phys. Rev. Lett.* **103**, 136403.
- Ni, Z. H., L. A. Ponomarenko, R. R. Nair, R. Yang, S. Anissimova, I. V. Grigorieva, F. Schedin, Z. X. Shen, E. H. Hill, K. S. Novoselov, and A. K. Geim, 2010, arXiv:1003.0202.
- Nieto, M. M., and P. L. Taylor, 1985, *Am. J. Phys.* **53**, 234.
- Nomura, K., and A. H. MacDonald, 2007, *Phys. Rev. Lett.* **98**, 076602.
- Novikov, D. S., 2007a, *Phys. Rev. B* **76**, 245435.
- Novikov, D. S., 2007b, *Appl. Phys. Lett.* **91**, 102102.
- Novoselov, K., A. Geim, S. Morozov, D. Jiang, M. Katsnelson, I. Grigorieva, S. Dubonos, and A. Firsov, 2005a, *Nature* **438**, 197.
- Novoselov, K. S., A. K. Geim, S. V. Morozov, D. Jiang, Y. Zhang, S. V. Dubonos, I. V. Grigorieva, and A. A. Firsov, 2004, *Science* **306**, 666.
- Novoselov, K. S., D. Jiang, T. Booth, V. V. Khotkevich, S. M. Morozov, and A. K. Geim, 2005b, *Proc. Natl. Acad. Sci.* **102**, 10451.
- Novoselov, K. S., Z. Jiang, Y. Zhang, S. V. Morozov, H. L. Stormer, U. Zeitler, J. C. Maan, G. S. Boebinger, P. Kim, and A. K. Geim, 2007, *Science* **315**, 1379.
- Ostrovsky, P. M., I. V. Gornyi, and A. D. Mirlin, 2006, *Phys. Rev. B* **74**, 235443.
- Ostrovsky, P. M., I. V. Gornyi, and A. D. Mirlin, 2007, *Eur. Phys. J. Special Topics* **148**, 63.
- Pedersen, T. G., 2003, *Phys. Rev. B* **67**, 113106.
- Peierls, R., 1979, *Surprises in Theoretical Physics* (Princeton University Press).
- Pereira, V. M., and A. H. Castro Neto, 2009, *Phys. Rev. Lett.* **103**, 046801.
- Pereira, V. M., A. H. Castro Neto, and N. M. R. Peres, 2009, *Phys. Rev. B* **80**, 045401.
- Pereira, V. M., F. Guinea, J. M. B. L. dos Santos, N. M. R. Peres, and A. H. Castro Neto, 2006, *Phys. Rev. Lett.* **96**, 036801.
- Pereira, V. M., J. Nilsson, and A. H. Castro Neto, 2007, *Phys. Rev. Lett.* **99**, 166802.
- Pereira, V. M., J. M. B. L. dos Santos, and A. H. Castro Neto, 2008, *Phys. Rev. B* **77**, 115109.
- Peres, N. M. R., 2009, *Europhysics News* **40**, 17.
- Peres, N. M. R., and E. V. Castro, 2007, *J. Phys.: Condens. Matter* **19**, 406231.
- Peres, N. M. R., F. Guinea, and A. H. Castro Neto, 2006, *Phys. Rev. B* **73**, 125411.
- Peres, N. M. R., F. D. Klironomos, S.-W. Tsai, J. R. Santos, J. M. B. L. dos Santos, and A. H. C. Neto, 2007a, *Europhys. Lett.* **80**, 67007.
- Peres, N. M. R., J. M. B. Lopes dos Santos, and T. Stauber, 2007b, *Phys. Rev. B* **76**, 073412.
- Peres, N. M. R., R. M. Ribeiro, and A. H. C. Neto, 2010, *Phys. Rev. Lett.* **105**, 055501.
- Peres, N. M. R., J. N. B. Rodrigues, T. Stauber, and J. M. B. L. dos Santos, 2009a, *J. Phys.: Condens. Matt.* **21**, 344202.
- Peres, N. M. R., and T. Stauber, 2008, *Int. J. Mod. Phys. B* **22**, 2529.
- Peres, N. M. R., T. Stauber, and A. H. Castro Neto, 2008, *Europhys. Lett.* **84**, 38002.
- Peres, N. M. R., L. Yang, and S.-W. Tsai, 2009b, *New J. Phys.* **11**, 095007.
- Pi, K., K. M. McCreary, W. H. W. Bao, Y. F. Chiang, Y. Li, S.-W. Tsai, C. N. Lau, and R. K. Kawakami, 2009, *Phys. Rev. B* **80**, 075406.
- Poirier, W., and F. Schopfe, 2010, *Nature Materials* **5**, 171.
- Polini, M., R. Asgari, Y. Barlas, T. Pereg-Barnea, and A. MacDonald, 2007, *Solid State Commun.* **143**, 58.
- Polini, M., A. Tomadin, R. Asgari, and A. H. MacDonald, 2008, *Phys. Rev. B* **78**, 115426.
- Ponomarenko, L. A., R. Yang, T. M. Mohiuddin, S. M. Morozov, A. A. Zhukov, F. Schedin, E. W. Hill, K. S. Novoselov, M. I. Katsnelson, and A. K. Geim, 2009, *Phys. Rev. Lett.* **102**, 206603.
- Rabi, I. I., 1928, *Z. Phys.* **49**, 507.
- Recher, P., B. Trauzettel, A. Rycerz, Y. M. Blanter, C. W. J. Beenakker, and A. F. Morpurgo, 2007, *Phys. Rev. B* **76**, 235404.
- Ribeiro, R. M., V. M. Pereira, N. M. R. Peres, P. R. Briddon, and A. H. Castro Neto, 2009, *New J. Phys.* **11**, 115002.
- Riedl, C., C. Coletti, T. Iwasaki, A. A. Zakharov, and U. Starke, 2009, *Phys. Rev. Lett.* **103**, 246804.
- Robinson, J. P., H. Schomerus, L. Oroszlany, and V. I. Fal'ko, 2008, *Phys. Rev. Lett.* **101**, 196803.
- Rosenstein, B., M. Lewkowicz, H. C. Kao, and Y. Korniyenko, 2010, *Phys. Rev. B* **81**, 041416(R).
- Rossi, E., and S. Das Sarma, 2008, *Phys. Rev. Lett.* **101**, 166803.
- Sauter, F., 1931, *Z. Phys.* **69**, 742.
- Schedin, F., A. K. Geim, S. V. Morozov, D. Jiang, E. H. Hill, P. Blake, and K. S. Novoselov, 2007, *Nature Materials* **6**, 652.
- Schneider, G. F., S. W. Kowalczyk, V. E. Calado, G. Pandraud, H. W. Zandbergen, L. M. K. Vandersypen, and C. Dekker, 2010, *Nano Lett.* **10**, 3163.
- Schwierz, F., 2010, *Nature Nanotechnology* **5**, 487.
- Semenoff, G. W., 1984, *Phys. Rev. Lett.* **53**, 2449.
- Service, R. F., 2009, *Science* **324**, 875.
- Sheehy, D. E., and J. Schmalian, 2007, *Phys. Rev. Lett.* **99**, 226803.
- Sheehy, D. E., and J. Schmalian, 2009, *Phys. Rev. B* **80**, 193411.
- Shon, N. H., and T. Ando, 1998, *J. Phys. Soc. Jpn.* **67**, 2421.
- Shung, K. W., 1986, *Phys. Rev. B* **34**, 979.
- Shytov, A. V., M. I. Katsnelson, and L. S. Levitov, 2007, *Phys. Rev. Lett.* **99**, 236801.
- Silvester, P. P., and R. L. Ferrari, 1996, *Finite Elements for Electrical Engineers*, 3rd ed. (Cambridge).
- Slater, J. C., and N. H. Frank, 1969, *Electromagnetism* (Dover).
- Sometani, T., 2000, *Eur. J. Phys.* **21**, 549.
- Sprinkle, M., D. Siegel, Y. Hu, J. Hicks, P. Soukiassian, A. Tejada, A. Taleb-Ibrahimi, P. L. Fève, F. Bertran, C. Berger, W. A. de Heer, A. Lanzara, and E. Conrad, 2009, *Phys. Rev. Lett.* **103**, 226803.
- Stander, N., B. Huard, and D. Goldhaber-Gordon, 2009, *Phys. Rev. Lett.* **102**, 026807.
- Stauber, T., N. M. R. Peres, and A. H. Castro Neto, 2008a, *Phys. Rev. B* **78**, 085418.
- Stauber, T., N. M. R. Peres, and A. K. Geim, 2008b, *Phys. Rev. B* **78**, 085432.

- Stauber, T., N. M. R. Peres, and F. Guinea, 2007, *Phys. Rev. B* **76**, 205423.
- Suzuura, H., and T. Ando, 2002, *Phys. Rev. Lett.* **89**, 266603.
- Tan, Y.-W., Y. Zhang, K. Bolotin, Y. Zhao, S. Adam, E. Hwang, S. Das Sarma, H. L. Stormer, and P. Kim, 2007, *Phys. Rev. Lett.* **99**, 246803.
- Tapasztó, L., G. Dobrik, P. Lambin, and L. P. Biró, 2008, *Nature Nanotechnology* **3**, 397.
- Teague, M. L., A. P. Lai, J. Velasco, C. R. Hughes, A. D. Beyer, M. W. Bockrath, C. N. Lau, and N.-C. Yeh, 2009, *Nano Lett.* **9**, 2542.
- Tikhonenko, F. V., D. W. Horsell, R. V. Gorbachev, and A. K. Savchenko, 2008, *Phys. Rev. Lett.* **100**, 056802.
- Tikhonenko, F. V., A. A. Kozikov, A. K. Savchenko, and R. V. Gorbachev, 2009, *Phys. Rev. Lett.* **103**, 226801.
- Titov, M., 2007, *Europhys. Lett.* **79**, 17004.
- Titov, M., P. M. Ostrovsky, I. V. Gornyi, A. Schuessler, and A. D. Mirlin, 2010, *Phys. Rev. Lett.* **104**, 076802.
- Trushin, M., and J. Schliemann, 2008, *Europhys. Lett.* **83**, 17001.
- Tworzydło, J., B. Trauzettel, M. Titov, A. Rycerz, and C. W. J. Beenakker, 2006, *Phys. Rev. Lett.* **96**, 246802.
- Tzalenchuk, A., S. Lara-Avila, A. Kalaboukhov, S. Paolillo, M. Syväjärvi, R. Yakimova, O. Kazakova, T. J. B. M. Janssen, V. Falko, and S. Kubatkin, 2010, *Nature Nanotechnology* **5**, 186.
- Wallace, P. R., 1947, *Phys. Rev.* **71**, 622.
- Wang, X., L. Zhi, and K. Müllen, 2008, *Nano Lett.* **8**, 323.
- Wehling, T. O., M. I. Katsnelson, and A. I. Lichtenstein, 2009, *Phys. Rev. B* **80**, 085428.
- Wehling, T. O., S. Yuan, A. I. Lichtenstein, and M. I. Katsnelson, 2010, *Phys. Rev. Lett.* **105**, 056802.
- Wu, X., Y. Hu, M. Ruan, N. K. Madiomanana, J. Hankinson, M. Sprinkle, C. Berger, , and W. A. de Heer, 2009, *Appl. Phys. Lett.* **95**, 223108.
- Wu, X., Z. Tang, H. Wu, J. R. Cort, G. W. Buchko, Y. Zhang, Y. Shao, I. A. Aksay, J. Liu, and Y. Lin, 2010, *Small* **6**, 1205.
- Wunsch, B., T. Stauber, F. Sols, and F. Guinea, 2006, *New J. Phys.* **8**, 318.
- Xia, F., T. Mueller, Y. ming Lin, A. Valdes-Garcia, and P. Avouris, 2009, *Nature Nanotechnology* **4**, 839.
- Yang, L., J. Deslippe, C. Park, M. L. Cohen, , and S. G. Louie, 2009, *Phys. Rev. Lett.* **103**, 186802.
- Young, A. F., and P. Kim, 2009, *Nature Phys.* **5**, 222.
- Zhang, Y., V. W. Brar, C. Girit, A. Zettl, and M. F. Crommie, 2009, *Nature Phys.* **5**, 722.
- Zhang, Y., V. W. Brar, F. Wang, C. Girit, Y. Yayon, M. Panlasigui, A. Zettl, and M. F. Crommie, 2008, *Nature Phys.* **4**, 627.
- Zhang, Y., Y.-W. Tan, H. L. Stormer, and P. Kim, 2005, *Nature* **438**, 201.
- Zheng, Y., and T. Ando, 2002, *Phys. Rev. B* **65**, 245420.
- Zhu, W., V. Perebeino, M. Freitag, and P. Avouris, 2009, *Phys. Rev. B* **80**, 235402.
- Ziegler, K., 2007, *Phys. Rev. B* **75**, 233407.
- Ziman, J. M., 1979, *Principles of the Theory of Solids*, 2nd ed. (Cambridge University Press).